Title	Jet enhanced exhaust hood
Author(s)	Kulmala, Ilpo
Citation	VTT Report : VALB 317 VTT , 1998, pages 37.
Rights	This report may be downloaded for personal use only.

JET ENHANCED EXHAUST HOOD

Report VALB 317

Ilpo Kulmala

This study was funded by Finnish Work Environment Fund
(Työsuojelurahasto)

Tampere, Finland
10 September, 1998

MANUFACTURING TECHNOLOGY

A Work report	
B Public report	x
C Confidential report	

Title of report
Jet enhanced exhaust hood

Client/sponsor of project and order	Report No.
Finnish Technology Development Centre (Tekes), Finnish Work Environment Fund (Työsuojelurahasto)	VALB 317
Project Enhancement of local ventilation systems with the aid of jets	Project No. V6SU00411
Author(s) Ilpo Kulmala	No. of pages/appendices 37

Keywords
Numerical simulation, jet-reinforced exhaust, local ventilation

Summary
A two-dimensional jet-reinforced Aaberg hood was modelled using a mathematical model based on potential flow theory and with a CFD model using the standard k-e model for turbulence closure. The accuracy of the calculations was verified by air velocity and capture efficiency measurements. The comparisons show that, for normal operating conditions, the both models predicted the mean air flows in front of the hood well. However, the CFD model gave more realistic results in the jet flow region and also of the short-circuiting flow. Both models became increasingly inaccurate when the ratio of the supply jet momentum to the exhaust flow momentum increased. With appropriate approximations, the calculation times could be greatly reduced without significantly affecting the accuracy of the results. The jet enhancement proved to be a very efficient way to increase the effective control range of exhaust hoods. Controlled air movements can be created at distances which are two to three times larger than with conventional suction alone without increasing the exhaust flow rate.

Date Tampere 10 ___.September__.1998

Markku Lumme	Ilpo Kulmala	Seppo Enbom
Research Manager	Senior Research Scientist	Checked

Distribution:
Client, 1 copy
VTT Manufacturing Technology/VAL4, 20 copies
Finnish Work Environment Fund ,5 copies

VTT Manufacturing Technology
Safety Engineering
P.O. Box 1701
FIN-33101 Tampere, Finland

Phone: +358 3 316 3111
Telefax: +358 3 316 3499
E-mail: Ilpo.Kulmala@vtt.fi
WWW: http://www.vtt.fi/manu/safety

Foreword

This work is a part of the Finnish National CFD Technology Programme research project Free and Forced Convection. The aim of the research was to improve the utilization of CFD in the applications of heat and mass transfer and industrial ventilation. This research report belongs to the research study of local ventilation, where the main goals have been to improve the design methods and performance of local ventilation systems.

This study was funded by the Technology Development Centre Finland (TEKES) and by Finnish Work Environment Fund (Työsuojelurahasto).

Tampere, August 1998

Ilpo Kulmala

Table of contents

Nomenclature

b_0	width of jet nozzle
h	height of exhaust opening above bench surface
H	dimensionless height of exhaust opening above bench surface
$J(x)$	jet momentum per unit width
J_0	initial jet momentum at nozzle
p	height of jet nozzle above bench surface
q	exhaust flow rate per unit width
R	dimensionless distance in polar co-ordinates, $R=r/p$
r	distance in polar co-ordinates, $r=(x^2+y^2)^{1/2}$
S	dimensionless height of exhaust slot, $S=s/p$
s	height of exhaust slot
U, V	mean velocity components in the x and y directions
x, y	co-ordinates
$y_{1/2}$	width of a plane jet, equal to the distance from the jet centreline to the point at which the streamwise velocity is half of its centreline value
r	density
s	constant, equal to 7.67
Y	dimensionless stream function, y /q
y	stream function

1 Introduction

The air quality in industrial premises has a significant impact on the well-being of the workers and comfort of the working environment. In cases where airborne contaminants are the main cause of poor air quality, local ventilation is normally the most economical and effective method for contaminant control. For manual operations in particular, it is often the only way to reduce airborne contaminant concentrations in the worker's breathing zone to acceptable levels.

A traditional form of the local ventilation system is a local exhaust hood which sucks air from all directions, even clean air from behind the hood. This results in a rapid decrease in velocity with increasing distance from the hood face. Therefore, the plain exhaust hood has a very short effective range and the hood must be located very close to the contaminant source to be efficient, which may interfere with the technological processes. This lack of directionality may result in excessive exhaust flow rates with large source-to-hood distances and is a major drawback of local exhaust systems.

A potentially very effective way to increase the effective control range of local exhaust systems is to use high velocity jets directed perpendicular to the exhaust flow. The principle of the system and the streamlines generated by a slot exhaust hood reinforced by a two-dimensional jet are shown in Figure 1. A jet entrains air as it is issued at a relatively high velocity from a narrow slot to a direction perpendicular to the direction of the exhaust flow. When injection and exhaustion is combined in a correctly balanced ratio, controlled air movement can be obtained over much greater distances than is possible with conventional systems. These jet reinforced systems are known as Aaberg hoods after to their Danish inventor. The original construction was a radial jet flow issued from the perimeter of the hood's circular flange, but later two-dimensional slot hoods have also been developed and tested.

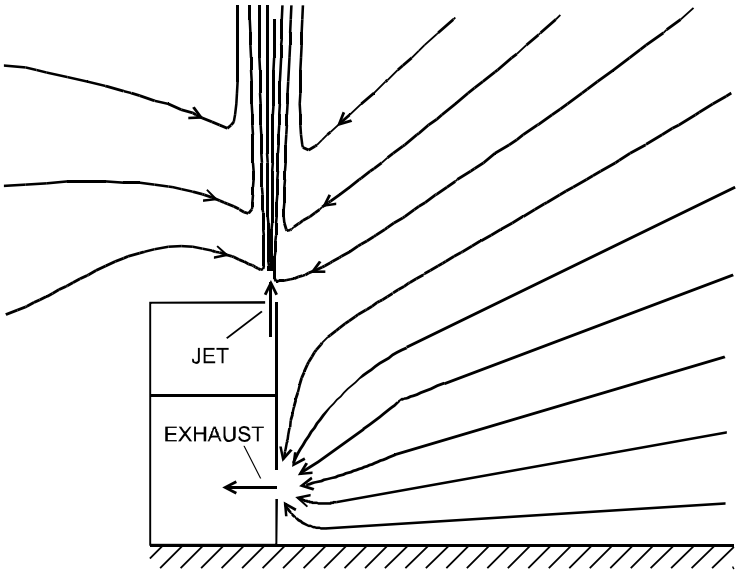

Figure 1. Jet enhanced exhaust hood.

In recent years, there has been much experimental research on jet enhanced local exhausts, first in Denmark (Hylgård 1987; Hogsted 1987; Germann, 1991) and later also in England (Saunders and Fletcher, 1993). These studies showed that the effective control range can be increased significantly by using assisting jets. However, for an optimum performance there should be a proper balance between injection and exhaustion. If the jet momentum was too weak the jet could be drawn into the suction opening whereas if it were too high, the effective suction area could be small although the capture distance might be large.

Theoretical models for the jet reinforced exhaust systems have been developed mainly at Leeds University. The first analytical model for a two-dimensional Aaberg hood was presented by Hunt and Ingham (1992). Later they also developed a more sophisticated numerical model which allows the geometry of the hood to be more accurately modelled (Hunt and Ingham, 1993). In this model, the flow field of a slot exhaust with two-dimensional wall-jet and free-jet was solved. The wall-jet model produced velocities which were reportedly in excellent agreement with experimental values. However, the free-jet model remained to be verified. Hunt and Ingham (1995) also presented an axisymmetric solution analogous in its formulation to the two-dimensional models. In all these models, turbulence is limited to the narrow jet region and the combination of the jet-induced and the exhaust flows is considered to be an inviscid potential flow.

The aim of this study was to investigate the accuracy of numerical simulations of jet reinforced exhaust systems and to extend the available information on the two-dimensional Aaberg hood. The studied case used a free plane jet for enhancing the exhaust flow. The modelling of the narrow supply jet together with the exhaust flow can cause convergence and stability problems and therefore suitable approximation methods were evaluated. The calculations were verified with air velocity and capture efficiency measurements. In addition, smoke tests were done in order to determine the operating conditions for the short-circuiting flow.

2 Experiments

2.1 Air flow measurements

The air velocities generated by the Aaberg exhaust hood were determined experimentally by laboratory measurements. The test set-up showing the cross-section of the exhaust hood is described in Figure 2. The exhaust hood and the supply jet plenum were made of plywood and they were located on a flat horizontal surface. The exhaust opening was a 5 cm wide slot made in a 0.27 m wide, 0.28 m high and 1 m long square duct. The jet was emerged from a slot of width 3.4 mm. The supply jet system was mounted with the front edge in line with the exhaust duct as shown in Figure 2. Vertical side walls of height 1.0 m and width 1.2 m were used at the both ends of the exhaust hood system to maintain the two-dimensionality of the flow.

The supply velocities used in the study were selected to represent velocities which are practically applicable. The exhaust flow rate was varied between 0.1 and 0.6 m^3/s and the supply

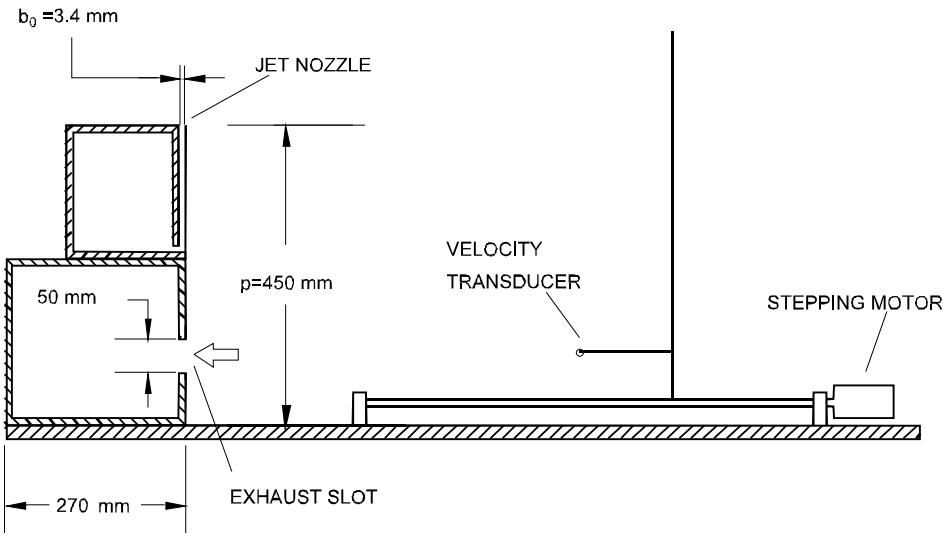

Figure 2. Experimental setup.

velocity between 11.7 and 23.5 m/s. The Reynolds number based on the width of the slot varied between 2700 - 5300. The different flow rates were adjusted using frequency controllers and measured by venturi tubes.

Air velocity measurements were taken with TSI Model 8465-075 velocity transducers connected to a computer for later analysis. Velocities were measured both in the jet region and on the centreline of the exhaust opening. The results were fed into a microcomputer, which was also automatically traversing the probe through predetermined coordinate points. At each measurement point, 3000 samples were recorded.

For flow visualization studies, smoke tubes were used to release smoke in the flow. The short-circuiting conditions of the flow were determined by varying the exhaust flow rate and measuring the supply air flow rate at which bending of the jet occurred.

2.2 Tracer gas measurements

A series of capture efficiency measurements were made under various operating conditions to determine the effective control range of the jet reinforced exhaust system. The tracer gas used was a neutrally buoyant mixture of sulphur hexafluoride (SF_6) and helium. Its release flow rate was kept constant by mass flow controllers (Bronkhorst type F201 C). Tracer gas was released through porous cylindrical diffusers of diameter 15 mm and length 23 mm. The tracer gas concentration was measured well downstream in the local exhaust duct by an IR-analyzer (Bomem). Measurements were made on a measurement grid on the vertical centre-plane of the exhaust system covering the area of capture efficiency of 0 to 100 %. The capture efficiency at each release point was determined by dividing the measured concentration by the concentration at 100 % capture, which was obtained by feeding tracer gas directly into the exhaust.

3 Numerical simulations

3.1 Potential flow model

The mathematical model for the two-dimensional Aaberg exhaust hoods presented by Hunt and Ingham (1993) is formulated in terms of the stream function ψ. In this model it is assumed that the stream function of the total flow is composed of the potential flows created by the suction and the jet induced flow. The resulting flow then satisfies Laplace's equation

$$\frac{\partial^2 \psi}{\partial x^2} + \frac{\partial^2 \psi}{\partial y^2} = 0 \tag{1}$$

For convenience, all lengths in the model are non-dimensionalized with respect to p and the stream function with the exhaust flow rate per unit length q. The dimensionless variables are thus

$$X = x / p,\ Y = y / p,\ R = r / p,\ \Psi = \psi / q \tag{2}$$

where r is the distance in polar co-ordinates and p is the height of the jet nozzle above the bench surface (Figure 3)

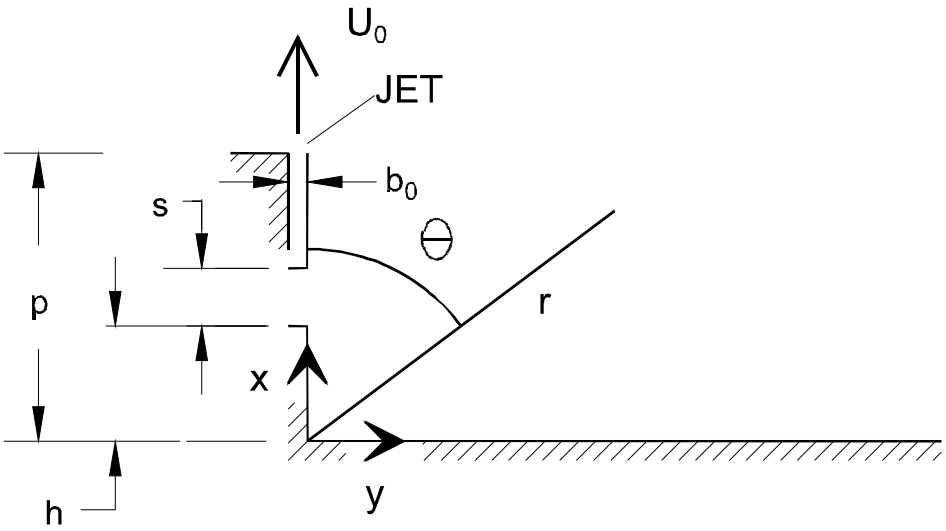

Figure 3. The geometry and the co-ordinate system of the mathematical model.

The injection of air is modelled as a two-dimensional turbulent jet. The stream function for the turbulent jet is determined analytically using boundary-layer theory and the solution is then used to find the value of the stream function at the edge of the jet boundary layer

$$\Psi_j = G_f\ (X - 1)^{1/2} \tag{3}$$

where G_f is the dimensionless operating parameter which is defined as

$$G_f = \frac{1}{2q}\left(\frac{3 b_0 U_0^2 p}{s}\right)^{1/2} \tag{4}$$

and where s=7.67 is an empirically determined constant. To facilitate the solving of the flow field, the jet is assumed to have zero thickness so that the boundary condition along the edge of the turbulent jet boundary layer, given by equation 3, is imposed along the x-axis.

Hunt and Ingham (1993) solved the boundary condition for Ψ for the flow far from the jet centreline by the method of separation of variables. It was assumed that the flow was a combination of the jet-induced and exhaust flows. This is given by

$$\begin{aligned}\Psi(R,\theta) = G_f \{ & \frac{R^{\lambda}}{\sin \lambda \frac{\pi}{2}} \sin\left[\lambda\left(\frac{\pi}{2} - \theta\right)\right] - \frac{\lambda R^{\lambda-1}}{\sin(\lambda-1)\frac{\pi}{2}} \sin\left[(\lambda-1)\left(\frac{\pi}{2} - \theta\right)\right] \\ & + \frac{1}{2!}\frac{\lambda(\lambda-1)R^{\lambda-2}}{\sin(\lambda-2)\frac{\pi}{2}} \sin\left[(\lambda-2)\left(\frac{\pi}{2} - \theta\right)\right] - \ldots\} + \left(1 - \frac{2\theta}{\pi}\right)\end{aligned} \tag{5}$$

where λ = 1/2 for the free-jet flow and $R=r/p$. At the open boundaries, the flow generated by the exhaust is thus approximated by a line sink.

The suction opening is modelled as a finite sized slot with a uniform velocity distribution. The solid bench surface and the vertical wall below the exhaust slot is a streamline of the flow through which the fluid does not cross and along this line Ψ=0. At the exhaust opening the face velocity is assumed to be constant. Between the slot and the jet, the vertical wall is also a streamline where the dimensionless stream function has value Ψ=1. The remaining boundary conditions are then

$$\begin{aligned} \Psi(0,Y) &= 0 \\ \Psi(X,0) &= 0,\ 0 < X < H \\ \Psi(X,0) &= (X - H)/S,\ H < X < H + S \\ \Psi(X,0) &= 1,\ H + S < X < 1 \\ \Psi(X,0) &= 1 + G_f\,(X - 1)^{\lambda},\ X > 1 \end{aligned} \tag{6}$$

where $H=h/p$ and $S=s/p$ is the dimensionless height of the slot above the bench surface and height of the slot, respectively.

Analytical solutions for appropriate boundary conditions are not possible so that numerical methods are the only means of solution. In this method, the area of integration of Laplace's equation is overlaid by a system of rectangular meshes, and an approximate solution to the differential equation is found at the mesh points. A central difference approximation of Equation 1 was used to calculate the stream function Ψ at a point (i,j) in a rectangular grid in terms of adjacent grid points

$$Y_{i,j} = \frac{Y_{i+1,j} + Y_{i-1,j} + Y_{i,j-1} + Y_{i,j+1}}{4} \tag{7}$$

This equation holds for interior points in the calculation domain and it can be used to write finite difference equations for each point where the stream function is not known. This yields as many simultaneous linear equations as there are unknowns. These equations were then solved using Gaussian elimination and the velocity components were calculated using central differences such that

$$\begin{aligned} U_{i,j} &= \frac{y_{i,j+1} - y_{i,j-1}}{2\Delta y} \\ V_{i,j} &= -\frac{y_{i+1,j} - y_{i-1,j}}{2\Delta x} \end{aligned} \tag{8}$$

where Δx and Δy are the mesh sizes in the x and y directions.

3.2 Viscous flow model

The flow field was also determined by solving the turbulent fluid flow equations using the k-ε model for turbulence closure. A commercial CFD program, FLUENT version 4.4, was used to predict the air flows. The air flow was assumed to be steady, two-dimensional and incompressible. In the simulations the QUICK differencing scheme was used for the discretization, and the solution algorithm was SIMPLE. Sufficient convergence was assumed to have occurred when the sum of successive fractional changes (residuals) was less than 10^{-4}.

The boundary conditions included a constant velocity u_0 and v_0 at the jet exit and at the hood face, and fixed pressure at the free-stream boundaries. At the free-stream boundaries the velocity components, pressure, and turbulence kinetic energy were unknown. They are also very difficult to determine accurately. Therefore, the fixed pressure boundary condition was used and pressure and turbulence kinetic energy were set to zero at these boundaries. The fixed pressure boundary condition allows the user to input the total pressure at a boundary instead of defining the velocity components. FLUENT then computes the normal velocity component and the static pressure at the boundary by applying Bernoulli's equation. However, this may lead to errors in the computational results if the boundaries are too close to the exhaust opening. The flow field was thus solved with different boundary locations to find the appropriate location of the boundaries. It was found that the results near the exhaust hood became independent of the boundary locations when the calculation domain size was 2.7 m in length and 1.7 m in height (Figure 4).

The assumption of a constant jet exit velocity is an approximation which is not quite accurate because the jet exit velocity profile was not uniform. Figure 5 shows the measured velocity profiles about 1 slot width downstream of the jet exit. It can be seen that the velocity profiles are nearly parabolic for the low Reynolds number flow, but that they become flatter as the jet exit velocity increases.

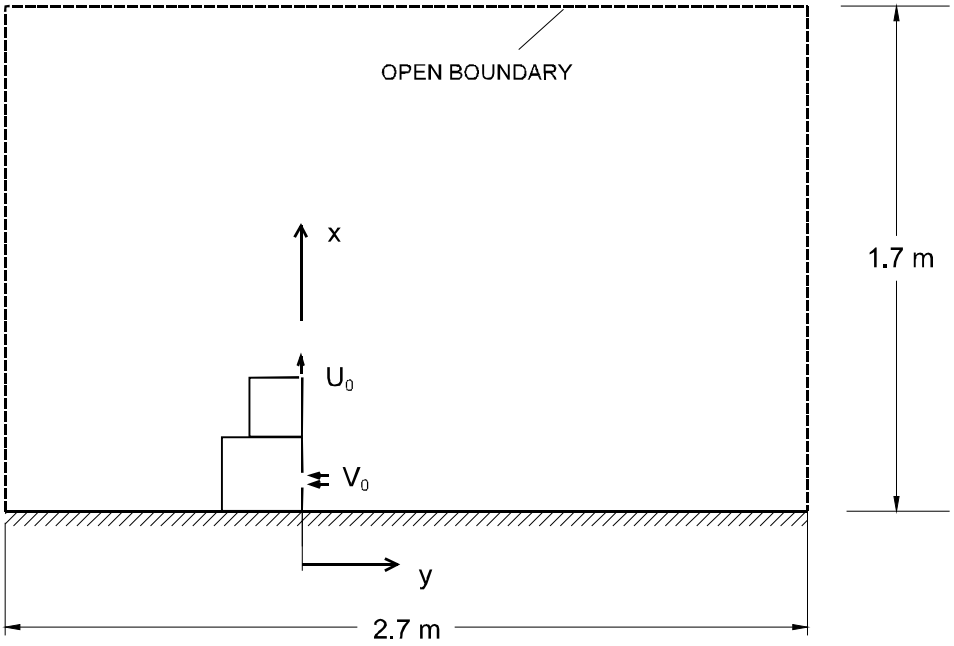

Figure 4. Boundary conditions and locations of the CFD model.

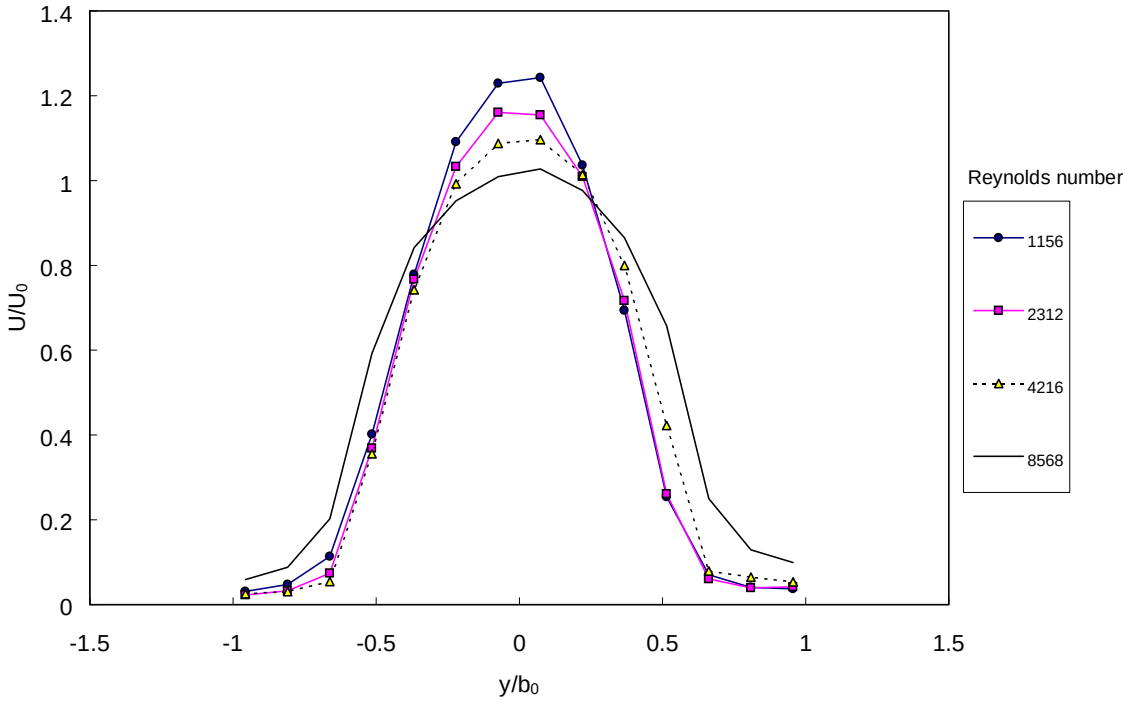

Figure 5. Measured jet velocity profiles with various supply velocities at $x/b_0=1$.

The calculations were done using a basic model and a modified model. In the basic model, the geometry and dimensions were similar to those used in the experiments, while in the modified model the width of the supply jet opening was varied. A non-uniform grid was employed with a finer grid spacing near the jet exit.

The grid-dependency was studied with the basic CFD model by solving the flow field with various grid sizes. The grid refinement tests were done using 52 x 51, 102 x 101, 202 x 200 and

402 x 398 grids. The corresponding number of grid points across the 3.4 mm wide jet opening was 1, 2, 4 and 8. The differences between the 102 x 101 and finer grids were so small that for the most of the calculations the 102 x 101 grid was used.

The narrow supply jet necessitates a very fine grid near the jet nozzle which results in a large grid aspect ratio far from the jet exit. This may cause stability problems and convergence difficulties. In practice, it is often necessary to obtain sufficiently accurate results by employing grids that are not excessively fine. Therefore, the calculations were also done for nozzle widths b_0 = 10 mm and 20 mm to study the effect of approximations on the flow patterns. In these approximations, it was not possible to simultaneously maintain both the jet supply flow rate and its momentum. Because the most important parameter in determining the jet flow is the initial momentum the jet, the velocity at the jet exit was based on constant momentum.

A common assumption is that sufficiently far from the nozzle the two-dimensional jet depends only on the initial momentum J_0 but not on the exact conditions of the jet generation. In the absence of pressure gradients and restricting surfaces, the integral of the streamwise momentum remains constant at its initial value

$$J = \rho \int_{-\infty}^{+\infty} U^2 dA = J_0 = \rho b_0 U_0^2 \tag{9}$$

To ensure the conservation of the momentum, the momentum across the jet at various locations downstream from the nozzle was calculated from the predicted velocities. The results showed that the calculations gave a momentum which was within 3 % of the initial value when two or more grid points was used across the jet. The momentum did not depend on the width of the jet nozzle so that one possible method for reducing the overall number of cells needed is to increase the initial width of the jet whilst keeping the initial momentum of the jet constant. Far downstream of the nozzle, this should produce the same flow pattern as with the actual jet nozzle width.

4 Results and discussion

4.1 Jet flow

The flow of a plane jet can be assumed to be consisting of a core region and a fully developed region. In the core region immediately downstream of the supply opening, the mixing of the jet fluid with the surroundings is not complete and the centreline velocity is constant. The length of the core region depends on the conditions at the nozzle exit but usually it extends to 5-10 opening widths. The extent of the potential core region tends to be smaller with a fully developed velocity profile than with a uniform flow (Schetz, 1984). Further downstream from the nozzle, the flow becomes fully turbulent. The centreline velocity decreases as the jet flow rate increases due to the entrainment of ambient air. The flow patterns become similar so that the velocity profile of the streamwise velocity component across the jet has the same shape at different distances from the supply opening.

The measured and calculated centreline velocity decay are shown in Figure 6. In a co-ordinate system where the x direction coincides with the jet axis with the origin at the exit, the centre-line velocity decay of the plane jet can be expressed by

$$\frac{U_{CL}}{U_0} = A\left(\frac{b_0}{x - x_0}\right)^{1/2} \tag{10}$$

where A is a constant and x_0 is the location of the virtual origin. A curve fit of the measured velocities gave A=2.6 and $x_0 = -b_0$ thus defining a virtual origin for the mean centreline velocity at 1 slot width upstream of the jet exit. The value of A is in fairly good agreement with the value of 2.4 recommended by Chen and Rodi (1980) after analyzing experimental data from various sources. The differences may be explained by the different initial conditions. The jet, upon leaving the nozzle, had a velocity profile typical of channel flows while in other investigations attempts were made to produce a uniform velocity profile. The different initial conditions are also most probably responsible for the shift in the location of the virtual origin.

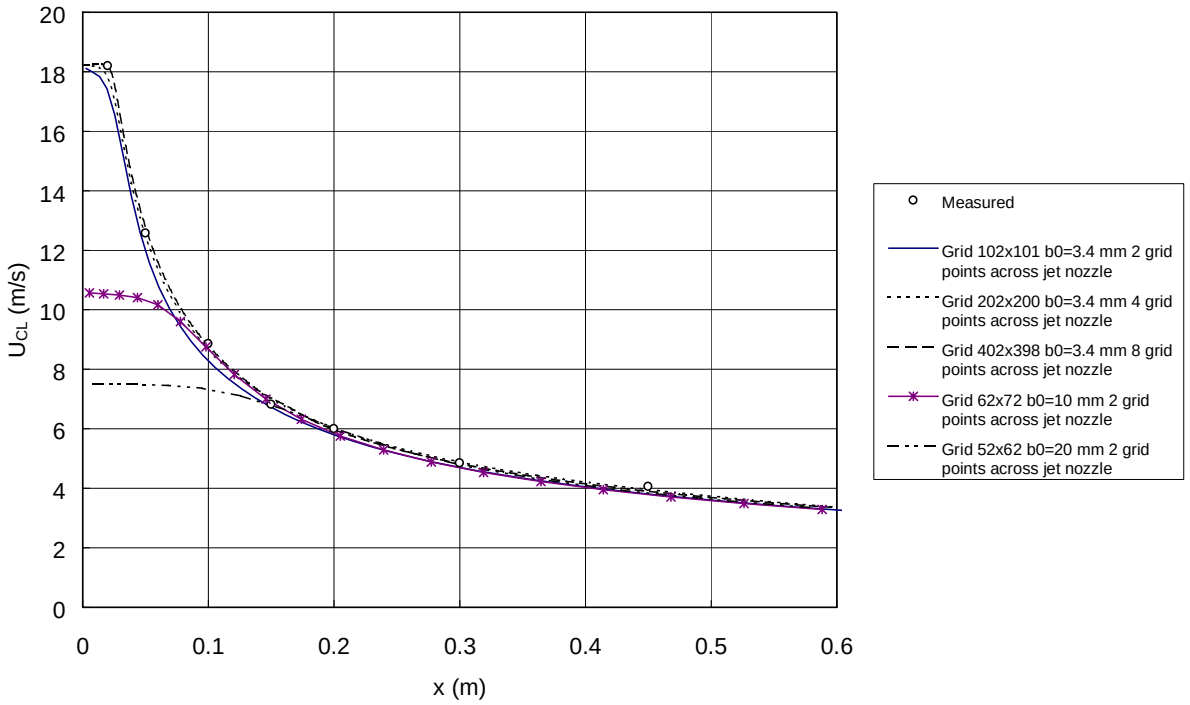

Figure 6. Measured and calculated mean velocity along the jet centre-line.

Figure 6 also shows the calculation results obtained both with the basic model using different grid sizes and with the modified models. With the basic model (b_0 = 3.4 mm), the centreline velocities are calculated fairly well when two or more grid points were used at the jet nozzle. With the modified models (b_0 = 10 and 20 mm) the velocities close to the jet exit were underestimated, as expected. However, at distances which are further than about 8 nozzle widths downstream from the jet exit the predicted velocities were in good agreement with the measured values.

The measured and calculated velocity profiles of the plane jet at different locations from the jet nozzle are shown in Figures 7 a-d. The experimental data for the fully developed region are presented in dimensionless form in Figure 8.

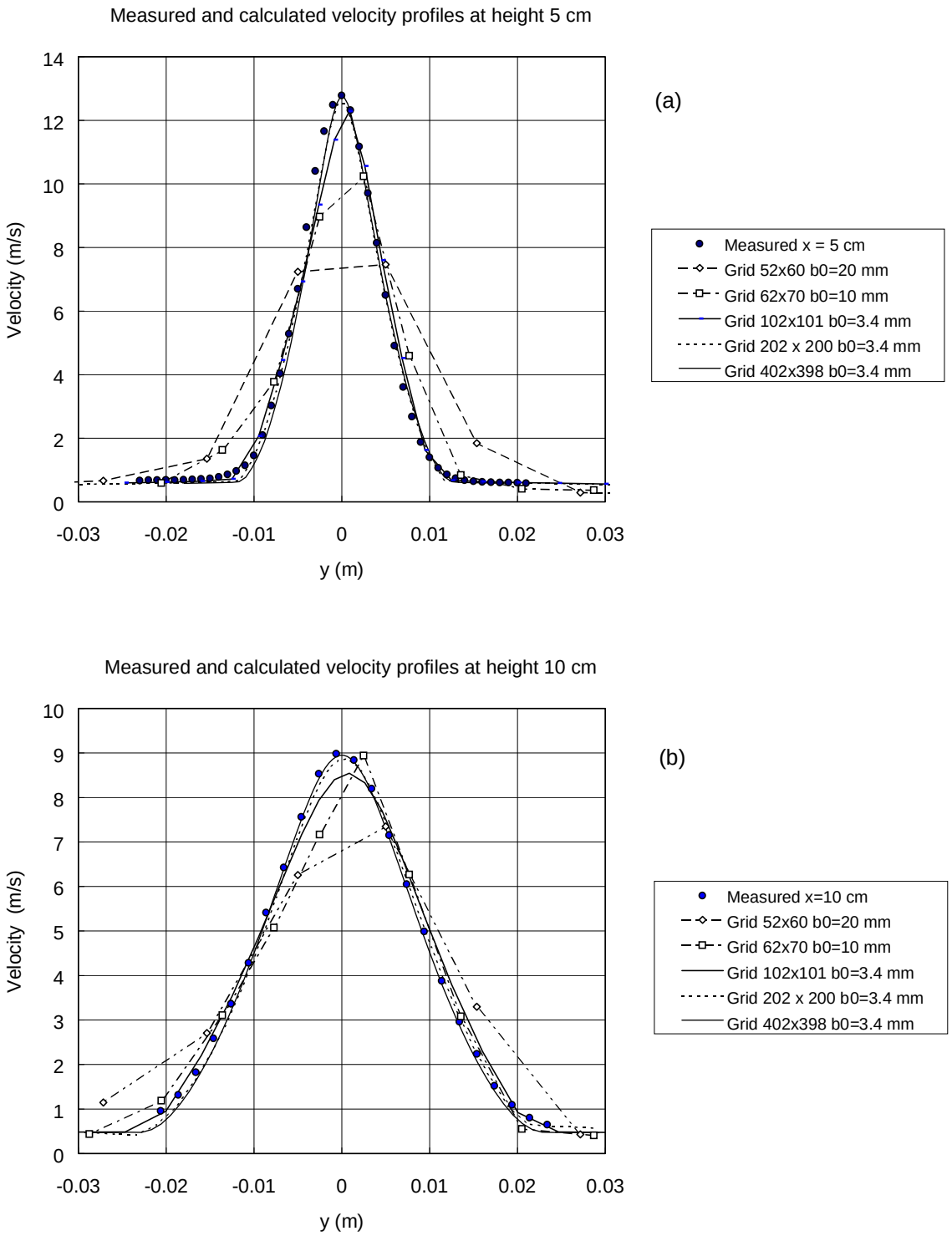

Figure 7. Velocity distribution across the plane jet.

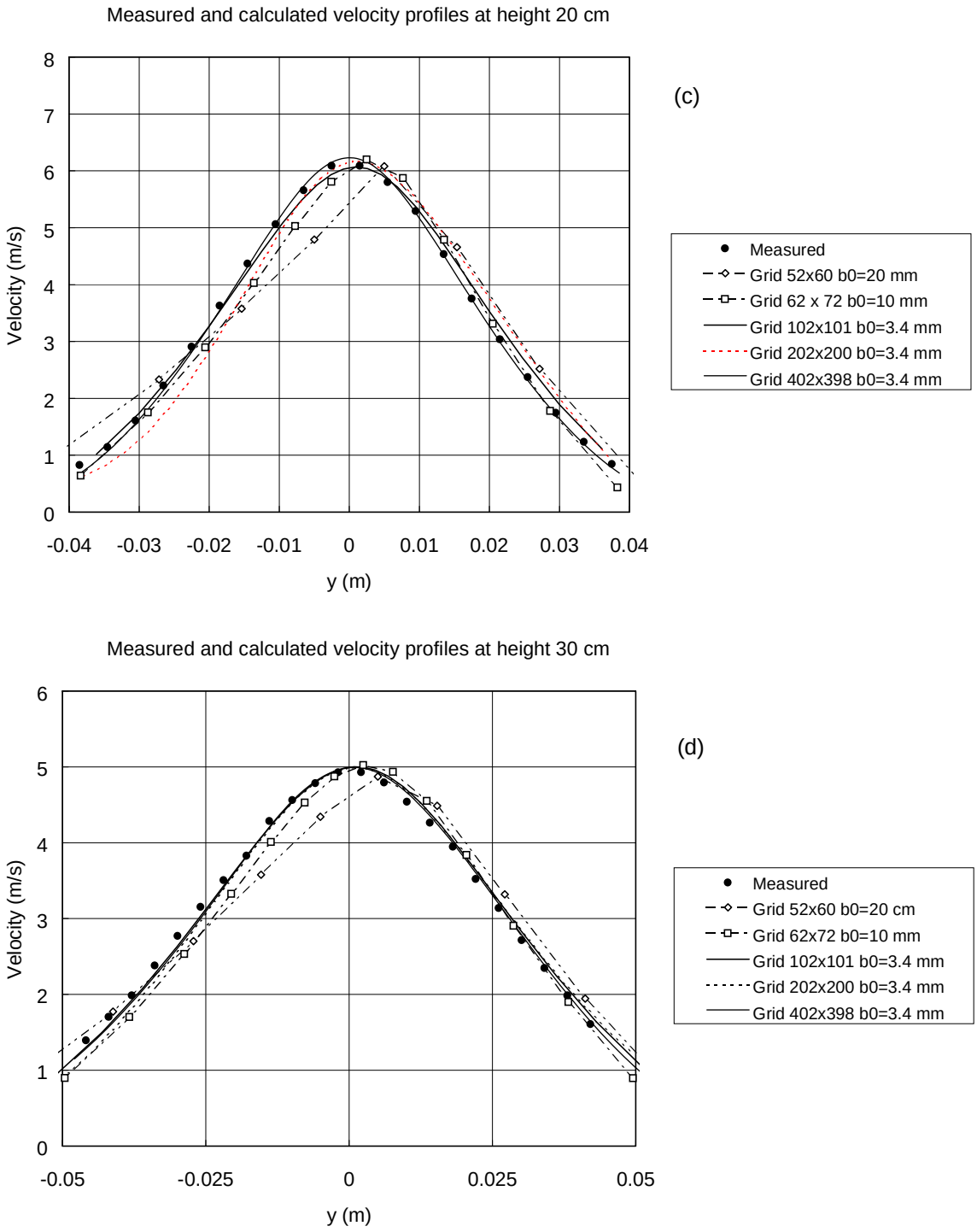

Figure 7 (continues). Velocity distribution across the plane jet.

It is seen that for reliable results near the jet exit, the nozzle width of the model should be the same as in the actual situation (Figure 7 a). Moreover, to obtain grid-independent results near the jet exit, very fine grids with at least four points across the jet are needed. Further downstream from the jet exit, the differences between the predictions and the measurements diminished even with the larger nozzle widths (Figures 7 c and d). The results thus confirm that at some distance downstream of the nozzle, the jet flow is independent of the exact exit condi-

tions and that the initial momentum of the jet is the most important parameter in determining the jet flow.

There is asymmetry in the calculated velocities about the jet centreline which can be clearly seen with the larger nozzle widths. This may be because of the asymmetric location of the nearby surfaces at the jet exit and because the horizontal distances from the jet to the open boundaries were not equal on both sides of the nozzle.

The measured velocity profiles normalized with the centreline values are plotted against *y/x* in Figure 8. It can be seen that the non-dimensional velocity profile can be described fairly well with a Gaussian profile. A least square fit to the data is

$$\frac{U(x,y)}{U_{CL}} = exp(-B(y/x)^2) \tag{11}$$

where B = 58. This is in good agreement with the value of B = 62 recommended by Chen and Rodi (1980).

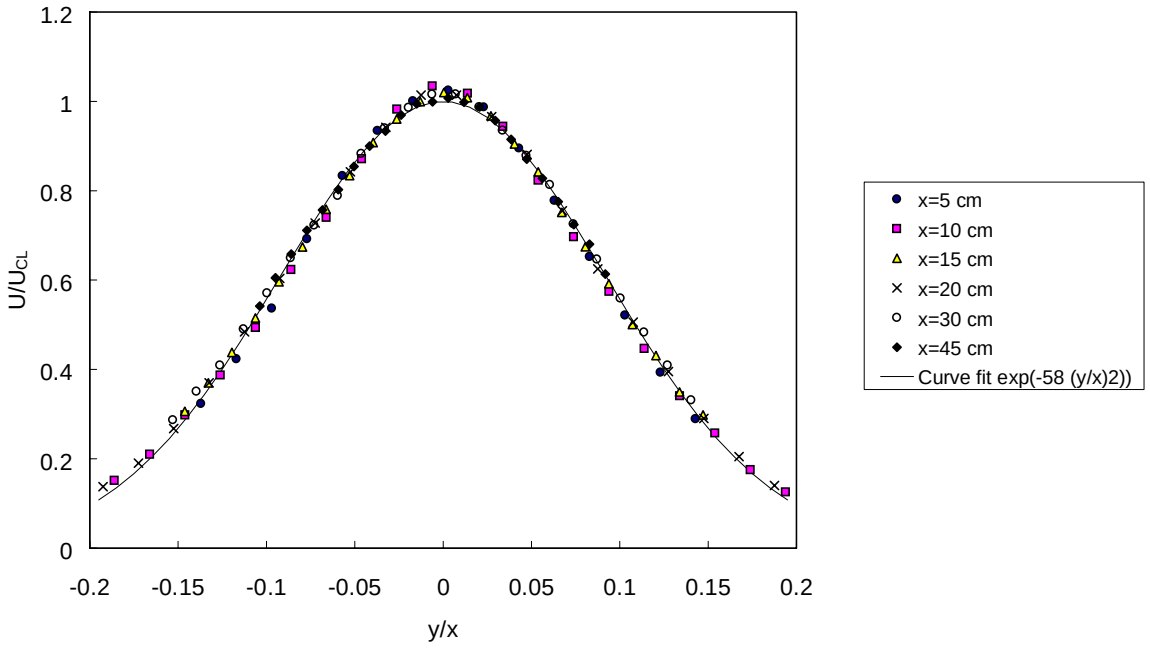

Figure 8. Measured velocity profile widths.

The air flow rate in the jet increases due to the entrainment of the ambient air. The air flow rate in the jet can be calculated using the mean velocity approximations in Equations 10 and 11:

$$q = \int_{-\infty}^{+\infty} U\,dy = A q_0 \left(\frac{\rho x}{B b_0}\right)^{1/2} \tag{12}$$

For the values A=2.6 and B=58, the volumetric air flow rate can thus be estimated by

$$q \approx 0.6\, q_0 \left(\frac{x}{b_0}\right)^{1/2} \tag{13}$$

This equation is plotted with the predicted air flow rates in Figure 9 when the supply flow rate q_0 = 0.062 m^3/s and b_0 = 3.4 mm. The flow rates calculated with larger nozzle sizes clearly overestimate the actual flow rate near the jet exit, but further downstream the differences become smaller. At distances greater than 0.3 m downstream of the jet exit, the predicted flow rates are very close to each other.

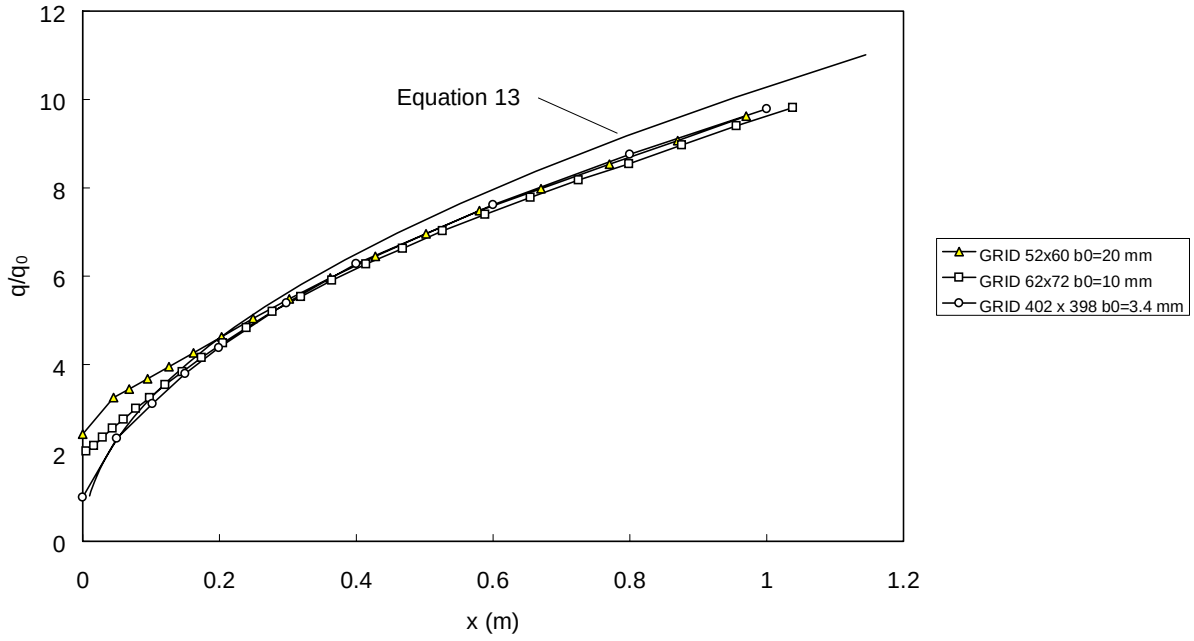

Figure 9. Calculated flow rate in the jet flow.

The growth of the jet with downstream distance is given in Figure 10 and compared with the calculated values. The jet spreads linearly with x and the locus of the half-velocity points is given by

$$y_{1/2} = 0.11x \tag{14}$$

This widening rate is typical to other data available in the literature, confirming that the jet was well behaved as far as mean-flow quantities are concerned. The widening rate is also very well predicted.

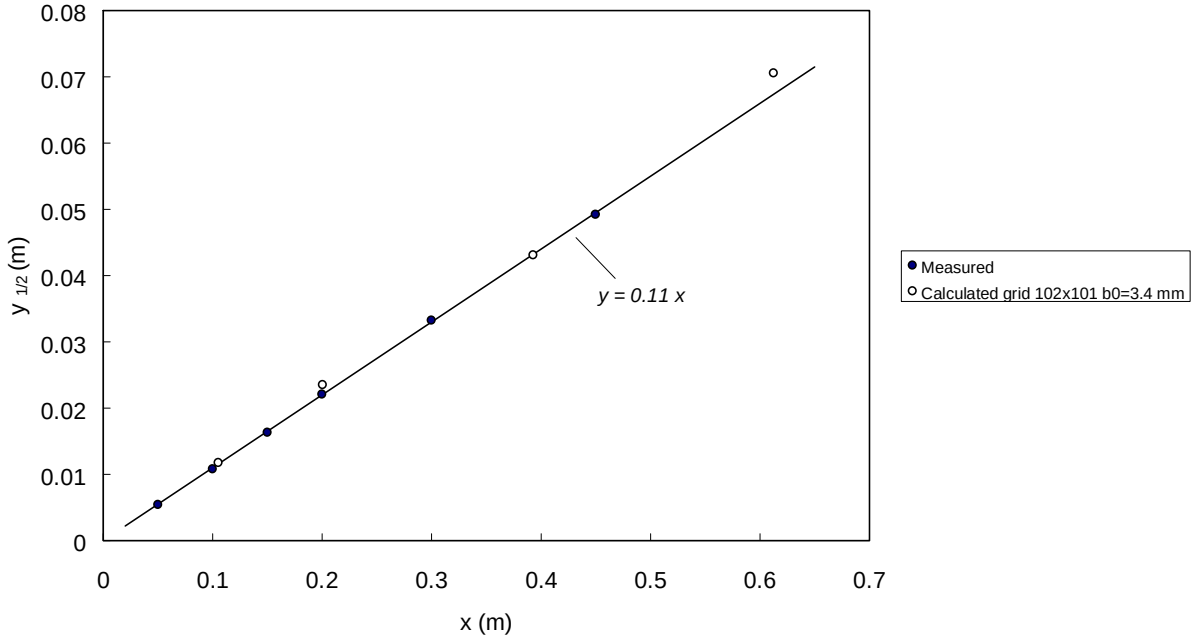

Figure 10. Predicted and measured growth of the jet with downstream distance.

4.2 Effect of the supply jet on the exhaust flow

The effect of injection of air on the airflow pattern was studied by calculating the flow fields under various operating conditions. The calculations were verified by measuring the air velocities in the centreline of the exhaust opening and the capture efficiencies. The changes in the value of the operating parameter G_f were achieved by varying the mean jet nozzle velocity, U_0, and exhaust flow rate, q, while keeping all other quantities constant.

The calculated stream functions, constant velocity contours and centreline velocities are shown in Figures 11 - 25. Each figure shows the predictions given by both the potential and viscous flow model. The distances in the figures are non-dimensionalized with respect to p, the height of the jet nozzle above the bench surface. The dimensionless streamlines are labelled by the fraction of total flow passing between that streamline and the bench surface. The velocities are presented as a fraction of the average hood face velocity and are calculated by

$$V_r = (U^2 + V^2)^{1/2} \tag{15}$$

Without the supply jet, the air is sucked from all directions into the exhaust opening and the velocities decrease rapidly with distance (Figures 11 and 12). In the potential flow model, the flow is produced by the slot in the corner of infinite right-angle walls. Sufficiently far from the opening, the velocities can be calculated by assuming the flow to be generated by a line sink. In the CFD-model, air also flows from behind the exhaust hood resulting in lower velocities in front of the hood. This is also seen in Figure 13 where the measured and calculated centreline velocities are compared.

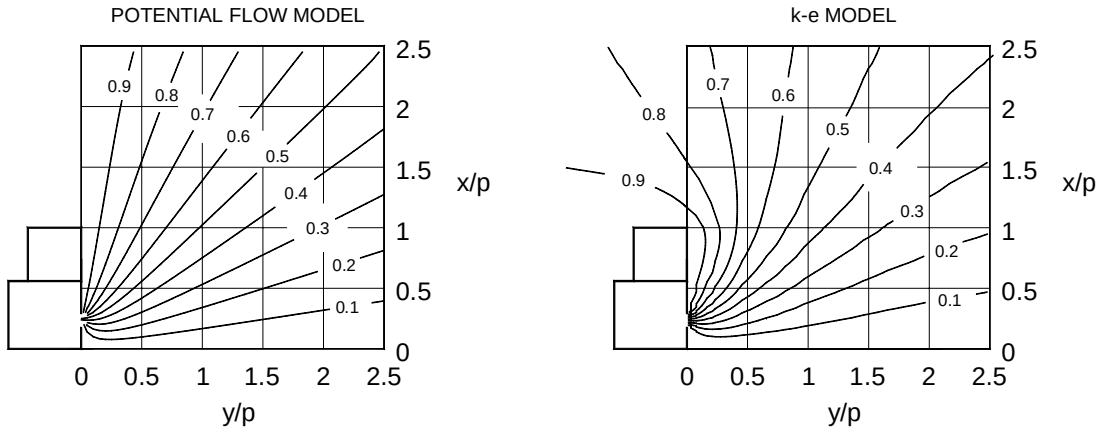

Figure 11. Predicted stream functions with the two models without supply jet.

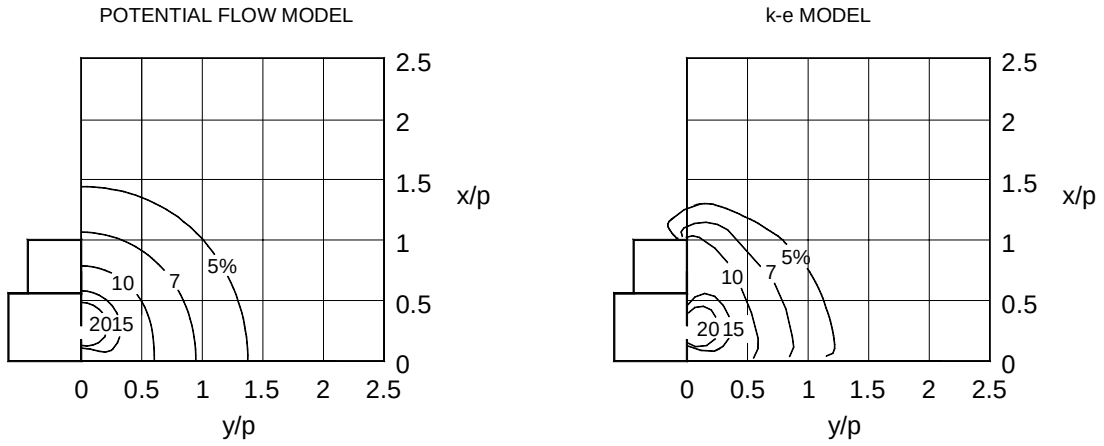

Figure 12. Predicted velocity contours with the two models without supply jet.

Injection of fluid changes the flow patterns remarkably as can be seen from the calculated stream functions and velocities in Figures 14 - 25. Combining exhaustion and injection creates two regions which are separated by a dividing streamline. At the dividing streamline, the dimensionless stream function has value $Y=1$. All streamlines between this dividing streamline and the bench surface enter the hood while above it air is entrained into the jet flow. If there were no dispersion, all neutrally buoyant gaseous contaminants released in the region where

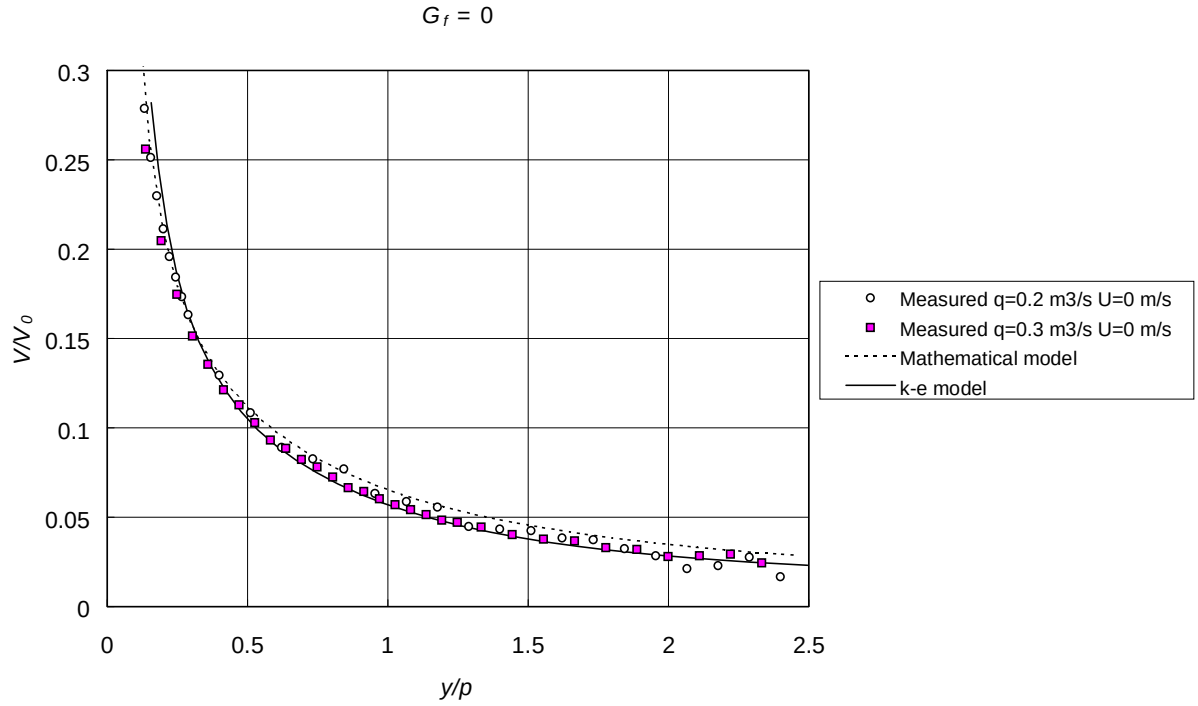

Figure 13. Measured and predicted centreline velocities without supply jet.

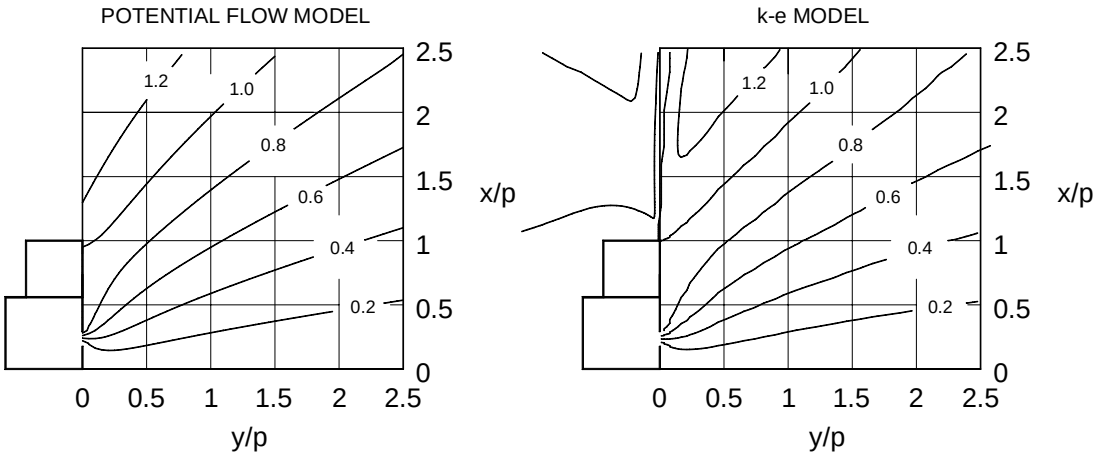

Figure 14. Predicted stream functions when G_f = 0.36.

Y <1 would enter the hood and be captured, whereas contaminants released outside this area would escape the hood.

The calculations predict that with G_f = 0.36, the injection effect is relatively small and the effective control area is large (Figure 14). As the value of the operating parameter G_f is increased, the dividing streamline Y =1, is forced towards the bench surface (Figures 17, 20 and

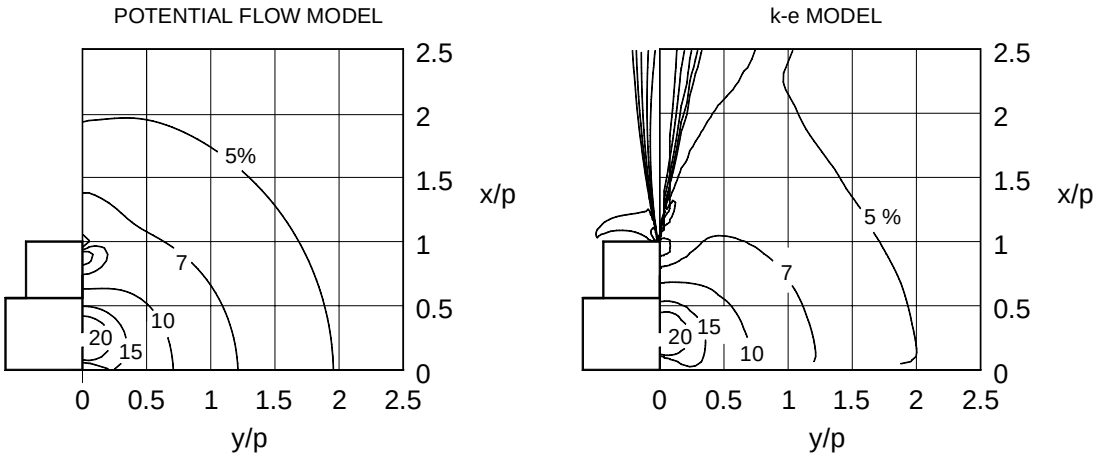

Figure 15. Predicted velocity contours when G_f = 0.36.

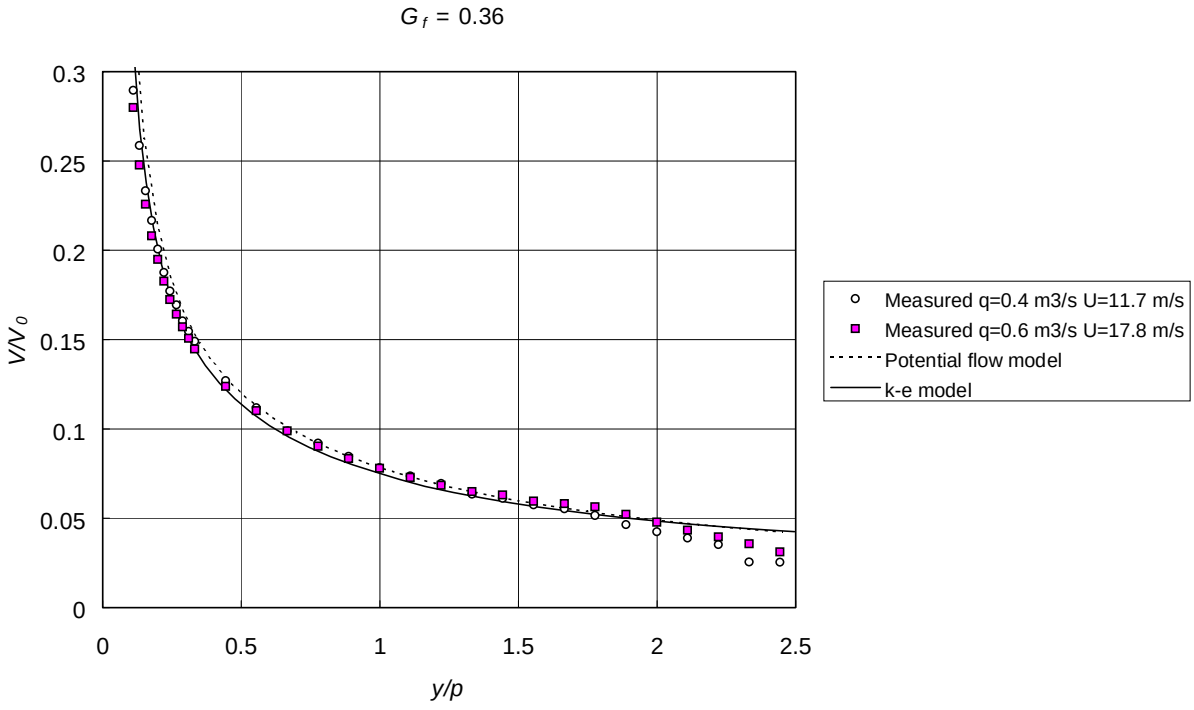

Figure 16. Measured and predicted centreline velocities when G_f = 0.36.

23). The displacement of the dividing streamline results in higher air velocities in front of the hood but at the same time the effective control area above the bench surface becomes narrower. The increase in velocities with injection is most profoundly felt at large distances from the hood as seen from the calculated velocity contours in Figures 12, 15, 18, 21 and 24. On

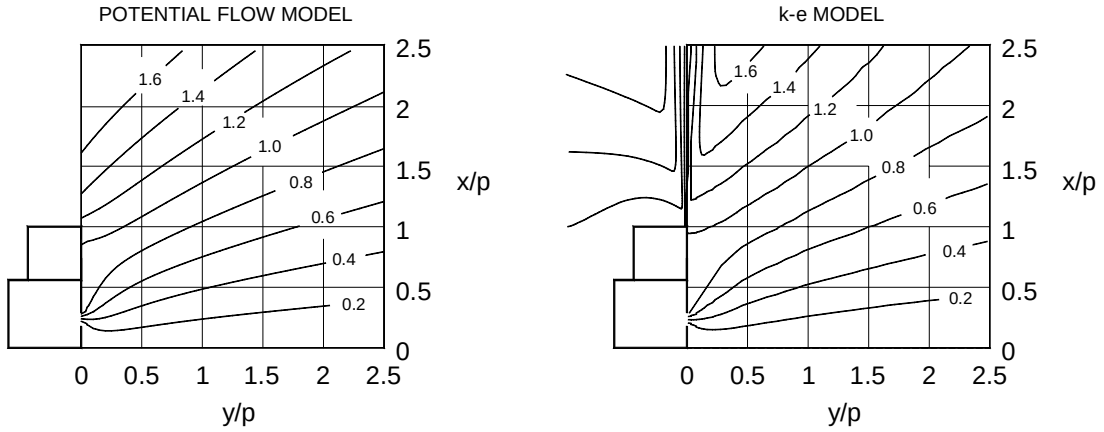

Figure 17. Predicted stream functions when $G_f = 0.74$.

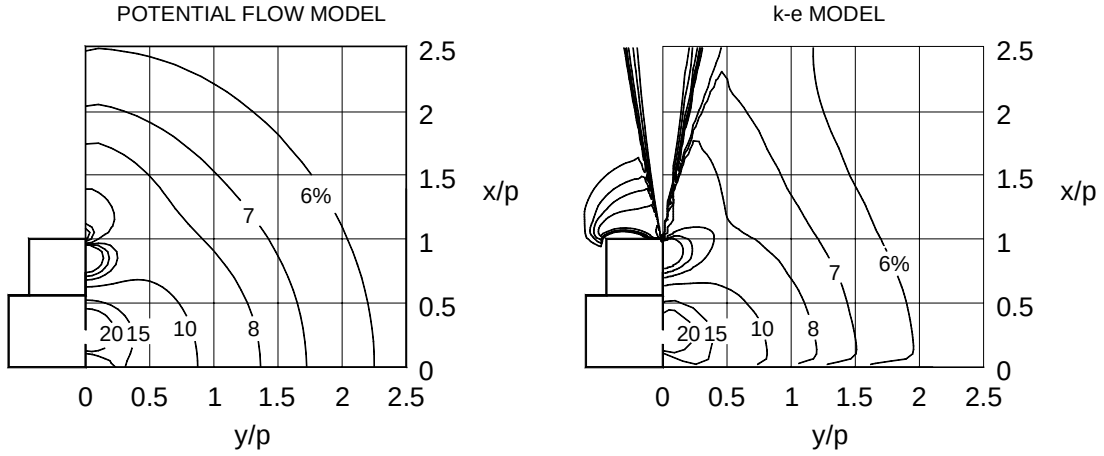

Figure 18. Predicted velocity contours when $G_f = 0.74$.

the other hand, in the region adjacent to the exhaust slot the velocity profiles remain almost unchanged indicating that the flow is dominated by the suction.

The agreement between the predicted and measured velocities was good for the operating parameter values *Gf* = 0, 0.36 and 0.74 (Figures 13, 16 and 19). However, the predictions became progressively more inaccurate as the operating parameter increased (Figures 22 and 25).

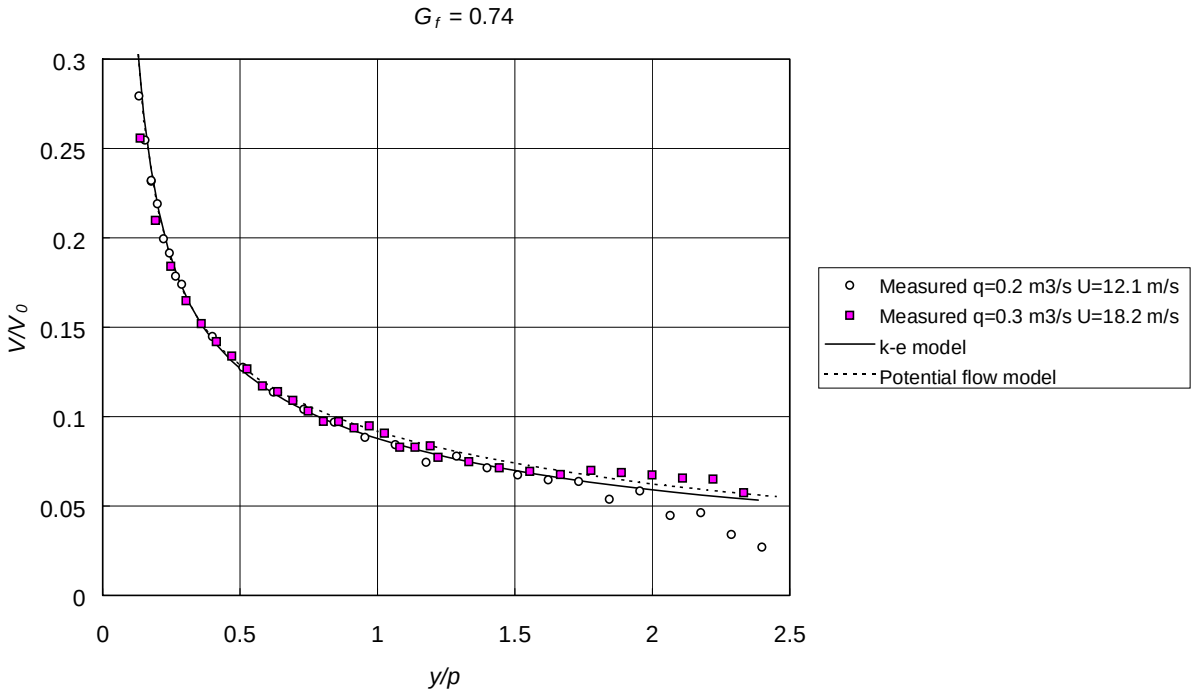

Figure 19. Measured and predicted centreline velocities when $G_f = 0.74$.

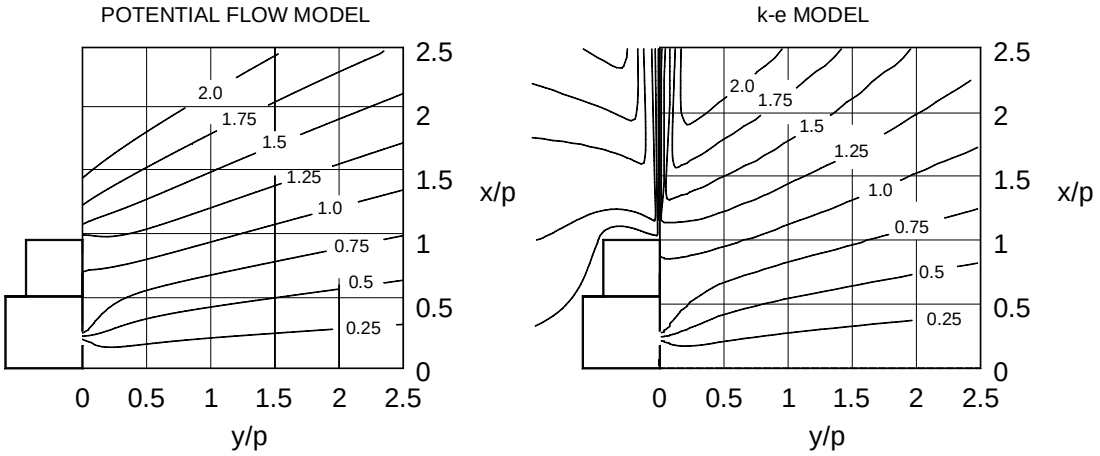

Figure 20. Predicted stream functions when $G_f = 1.44$.

The discrepancies are possibly because, in the actual situation, three-dimensional effects become important. The potential flow model produced higher values for the stream function at the jet boundaries than the viscous flow model and also clearly overestimated the velocities more than the viscous flow model. The qualitative agreement of streamlines and velocity contours produced by both models is good in front of the exhaust. They also predict similar behaviour as the value of the operating parameter G_f was varied. At greater distances above the

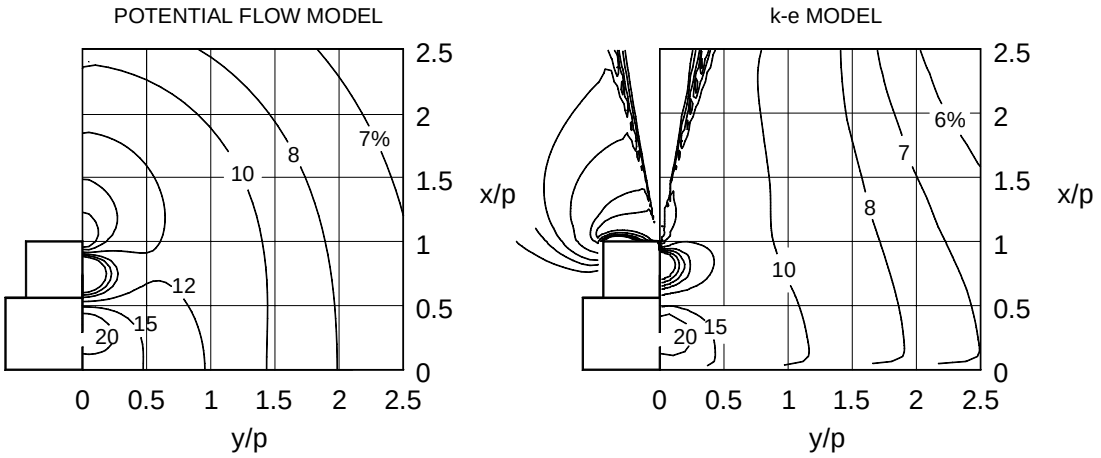

Figure 21. Predicted velocity contours when G_f = 1.44.

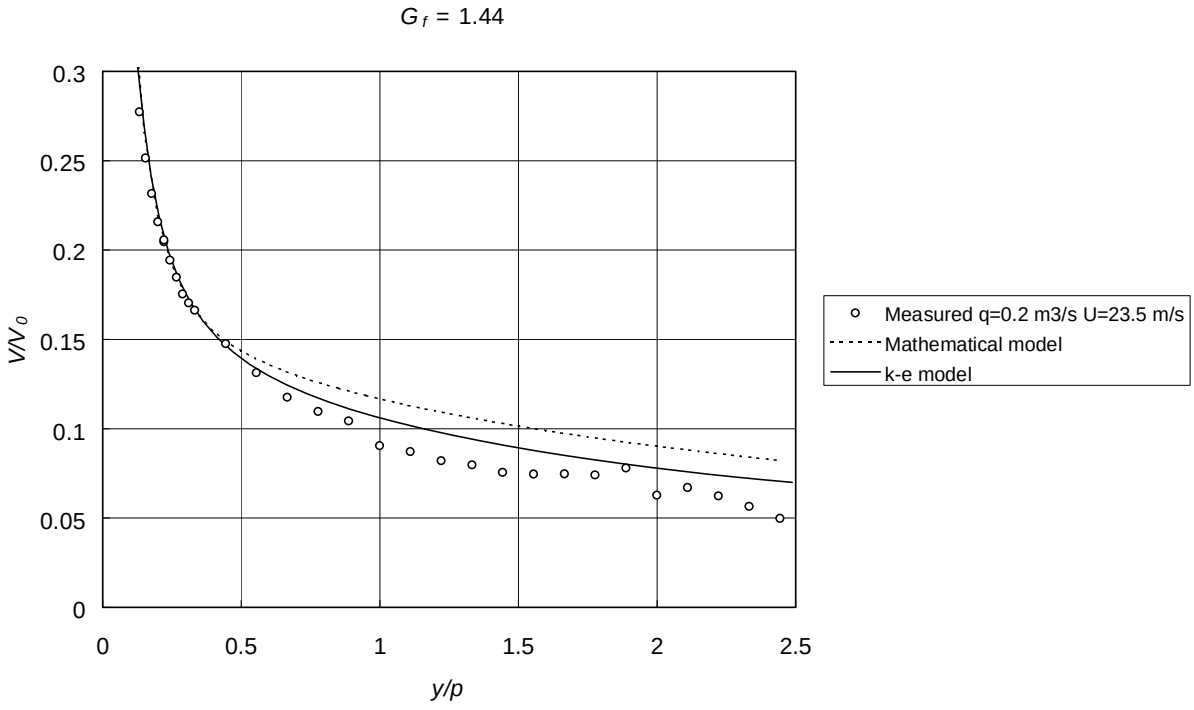

Figure 22. Measured and predicted centreline velocities when G_f=1.44.

bench surface, the velocity contours predicted by the mathematical model are more curved than in the CFD-model, which predicts more constant velocities in the vertical direction. The greatest differences are in the jet flow region where the potential flow model does not predict the velocities and stream function correctly.

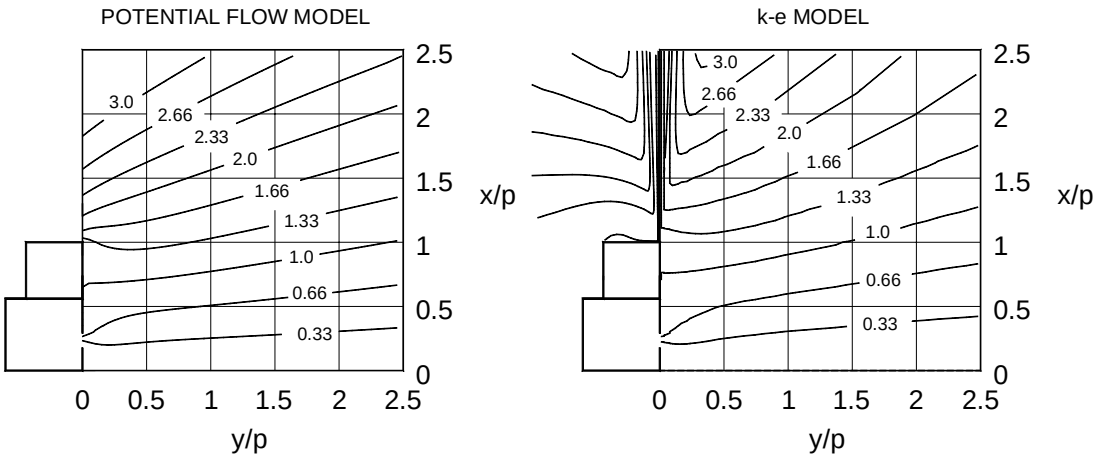

Figure 23. Predicted stream functions when G_f = 2.2.

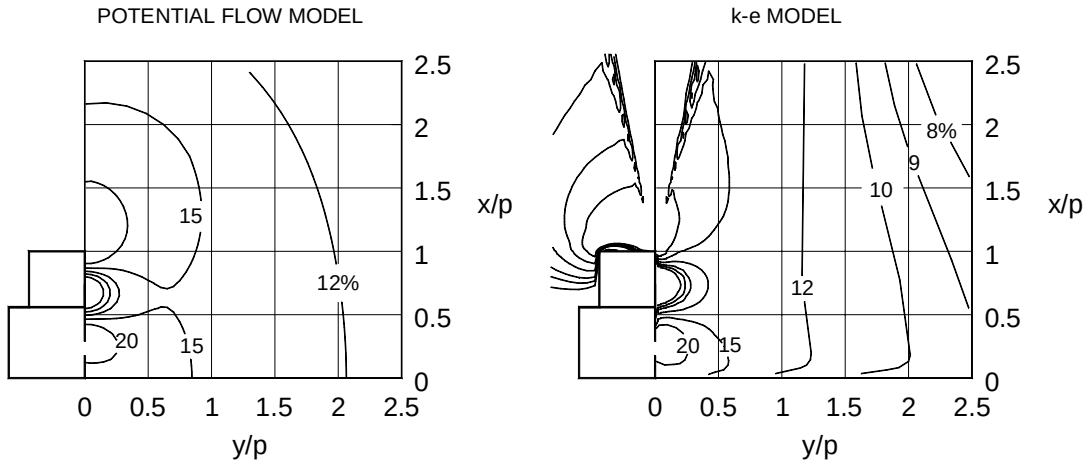

Figure 24. Predicted velocity contours when G_f = 2.2.

The hood centreline velocities in Figures 13, 16, and 19 were measured when varying the supply velocity and exhaust flow rate whilst keeping G_f constant. According to the theory, this should produce similar dimensionless velocities and this was confirmed by the experiments. The viscous flow calculations made for the same operating conditions also produced similar mean flow behaviour indicating that the dimensionless operating parameter G_f is the

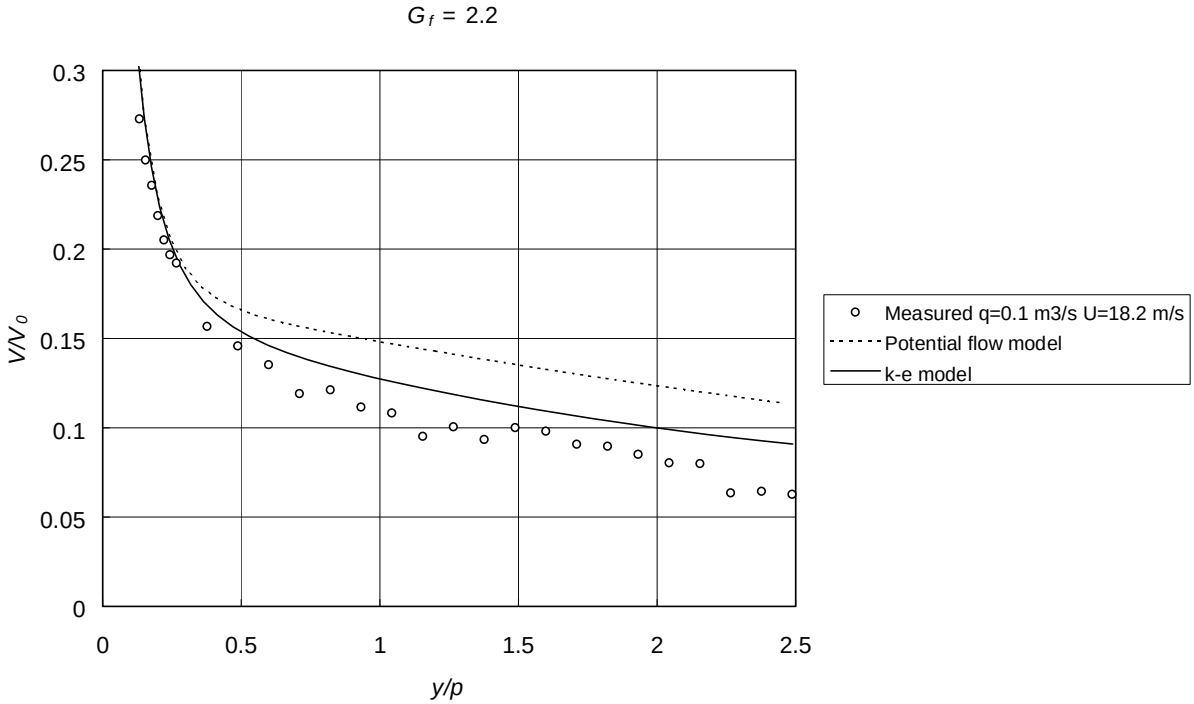

Figure 25. Measured and predicted centreline velocities when G_f = 2.2.

most important factor in characterizing the flow field of the two-dimensional jet enhanced exhaust system.

Without turbulent fluctuations, neutrally buoyant contaminants would follow the mean flow streamlines and the capture efficiency would be a step function with values 1 and 0. However, in reality turbulence causes dispersion around the mean flow streamlines and the capture efficiency changes more gradually. Assuming symmetric tracer gas distribution about the streamlines, the dividing streamline would correspond to the 50 % capture efficiency contour.

In order to determine the effective control range for the jet enhanced exhaust system in practise, capture efficiency measurements were made for various operating conditions. The results are shown in Figures 26 - 29 where the measured 10, 50 and 90 % capture efficiency contours are plotted. For comparison, the figures also show the dividing streamline predicted by the viscous flow model. It is seen that although there is scatter typical to tracer gas measurements the location of the 50 % capture efficiency curve corresponds satisfactorily with the predicted location of the dividing streamline.

It is important to notice that the region where the capture efficiency drops from 90 % to 10 % becomes wider as the distance from the hood increases. This is due to the increased time required for the contaminant to travel into the hood, which in turn causes greater dispersion around the streamlines (Flynn and Ellenbecker, 1986). The long capture times can also be caused by low velocities due to low exhaust flow rates. This was the case during the capture efficiency measurements with the values of G_f = 1.44 and G_f = 2.2 which were achieved with lower exhaust flow rates than in cases when G_f was 0.36 or 0.74. This increased dispersion is also reflected in wider capture efficiency contours (Figures 26 - 29).

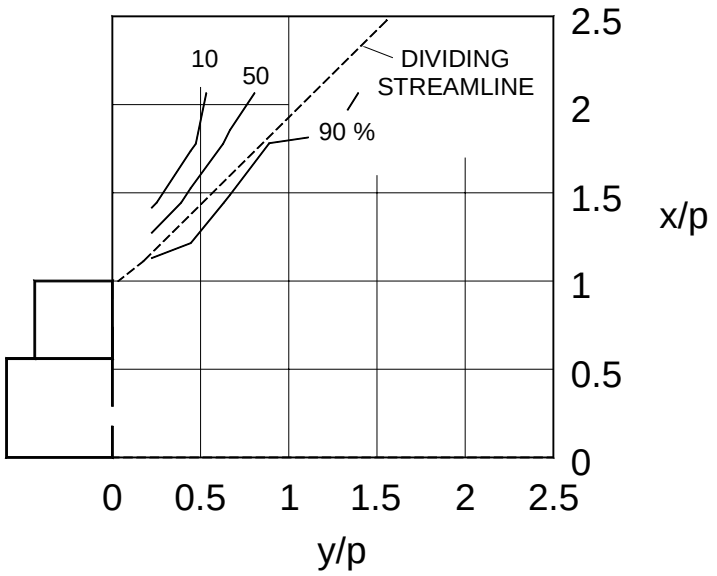

Figure 26. Measured capture efficiency contours and location of the CFD-predicted streamline when G_f = 0.36.

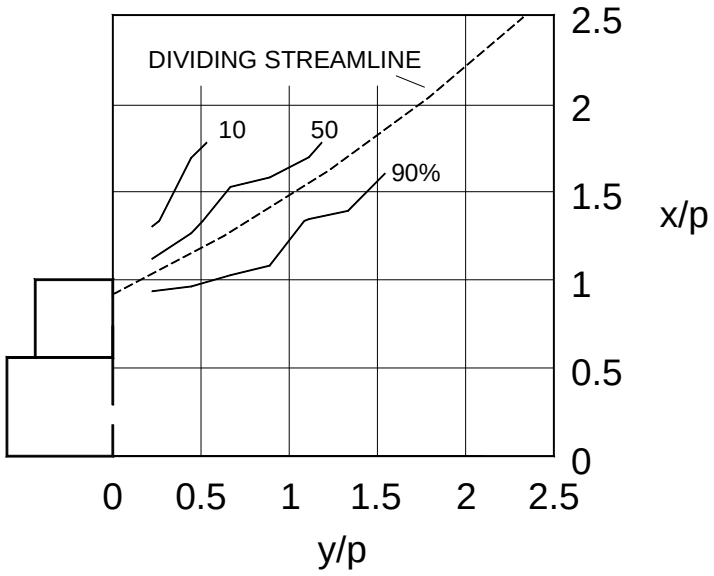

Figure 27. Measured capture efficiency contours and location of the CFD-predicted streamline when G_f = 0.74.

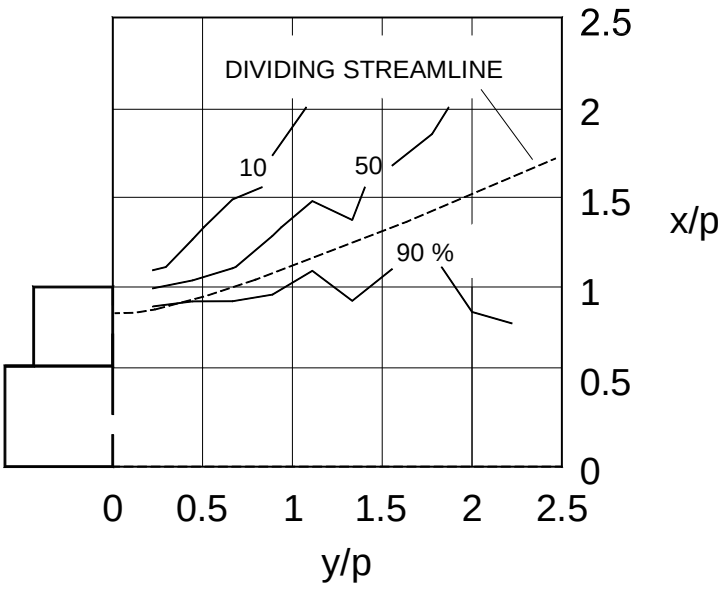

Figure 28. Measured capture efficiency contours and location of the CFD-predicted streamline when G_f = 1.44.

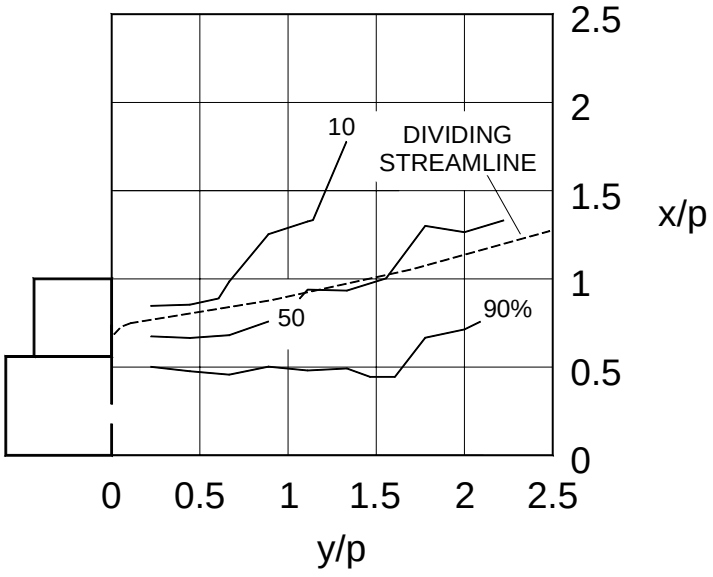

Figure 29. Measured capture efficiency contours and location of the CFD-predicted streamline when G_f = 2.2.

Increasing the value of G_f increases the velocities and the working range of the Aaberg exhaust hood. However, the spread of contaminants limits, in practise, the maximum value of the operating parameter G_f. This is in line with the observations made by Saunders and Fletcher (1993) who found that the capture distance first increases and then decreases with increasing jet velocity and hence the value of the operating parameter. It may thus be concluded that for an opti-

mum control of contaminants the operating parameter should not be too high. The optimum operating condition for a particular case depends on the geometry and the properties of the contaminant source but the results suggest that a good balance between the suction and injection is obtained with G_f = 0.74 - 2.2. With these values, the Aaberg hood can increase the distance where velocities are typical to those used for contaminant control over two to three times greater than possible when using conventional suction alone. This is a significant improvement making jet assisted exhaust an attractive choice in cases where the contaminant sources are large such as for open surface tanks. The long operating range is also very useful in cases where the conventional exhaust hood would disturb industrial operations or obstruct the worker's movements.

The models are restricted to cases where the flow is two-dimensional, and which may be difficult to realize in practise. This requires very long slot hoods or side walls at the end of the hood. In three-dimensional cases, the velocities decrease more rapidly than predicted by the two-dimensional model due to flow from the sides. The three-dimensional effects require further studies.

4.3 Comparison of the CFD models

The calculations with CFD models were made with different grid sizes and various widths of the jet nozzle to study the effect of approximations on the overall flow patterns. These calculations demonstrated that for small values of G_f the results are in good agreement with each other. The differences between the models became increasingly greater as the operating parameter increased.

Figures 30 and 32 show examples of the calculated streamlines for two values of G_f with various grid sizes. The corresponding velocity contours are plotted in Figures 31 and 33. It can be seen that the velocities and stream functions were quite similar when G_f = 0.74. The differences between the predictions became more clear when the value of G_f increased. When G_f = 2.2 the calculated streamlines with the models using larger nozzle widths located more sparsely than with the basic flow case. Further from the exhaust opening, the calculated velocities were also underestimated by about 20 % with a nozzle width b_0 = 20 mm, and about 10 % with b_0 = 10 mm compared to the basic case (b_0 = 3.4 mm).

With the basic model (b_0 = 3.4 mm), the calculated stream functions and velocity contours were altered only slightly when the grid size was doubled from the 102 x 101 to 202 x 200 indicating that the results were grid-independent.

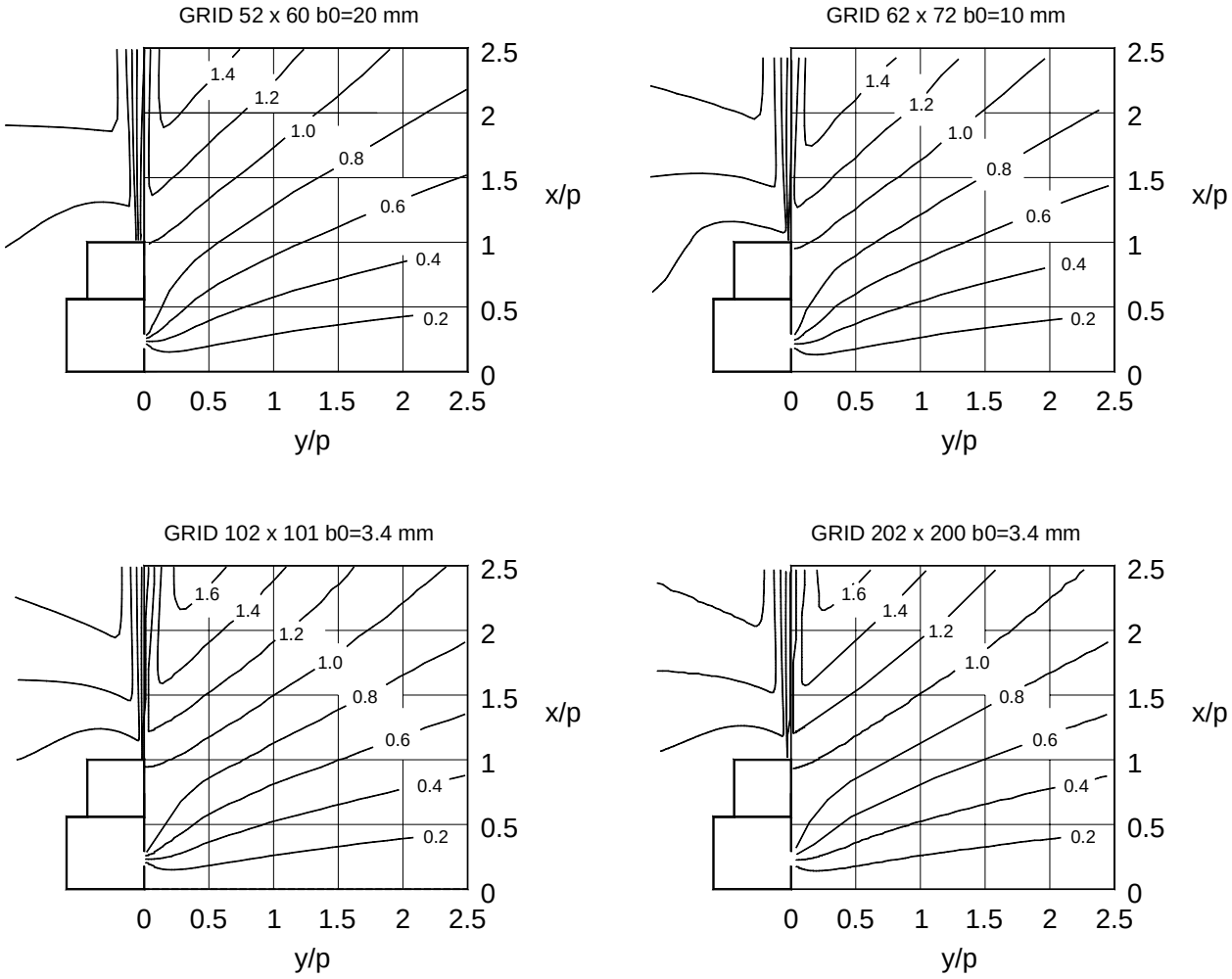

Figure 30. Calculated stream functions with various models when $G_f = 0.74$.

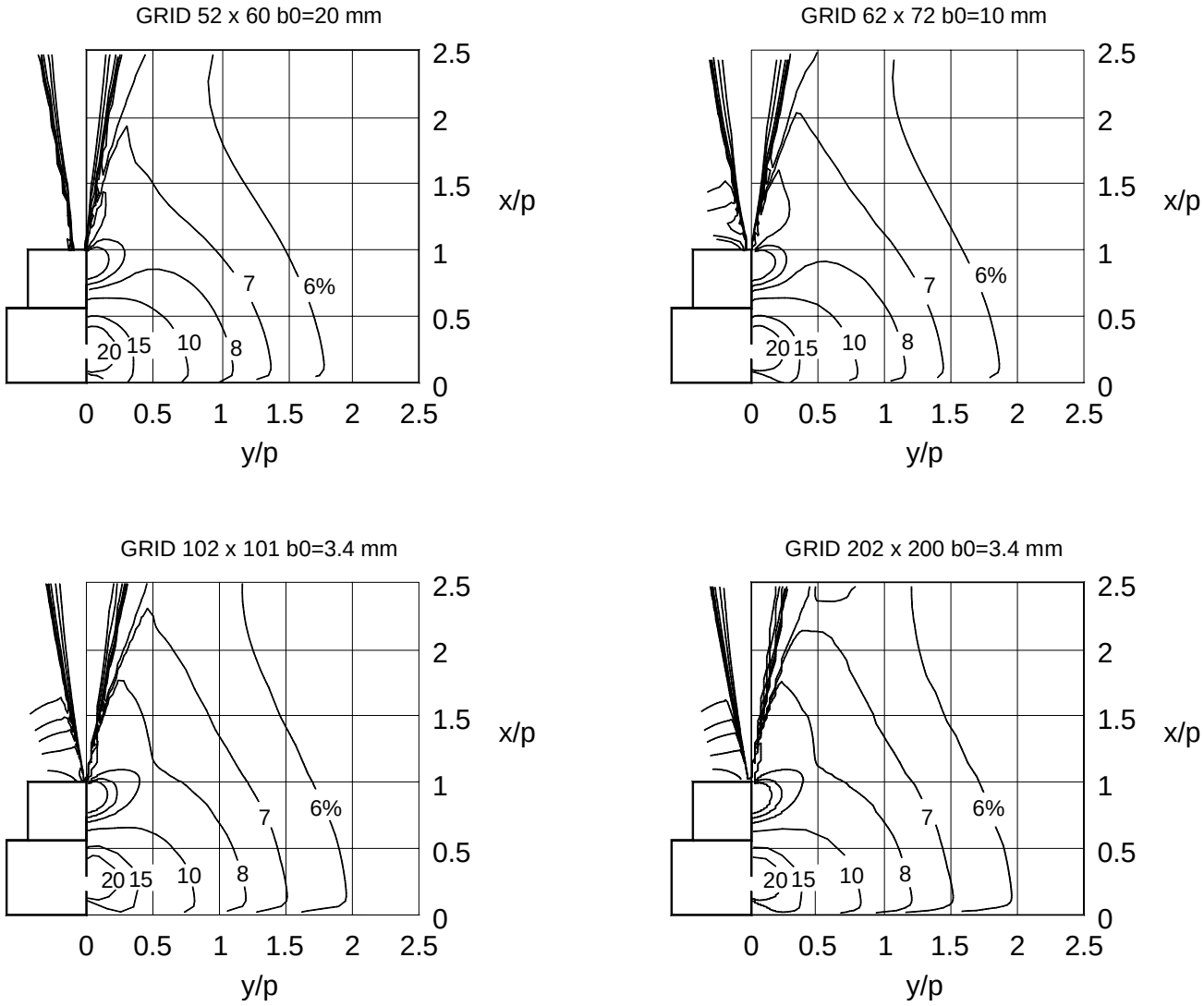

Figure 31. Calculated velocity contours with various models when $G_f = 0.74$.

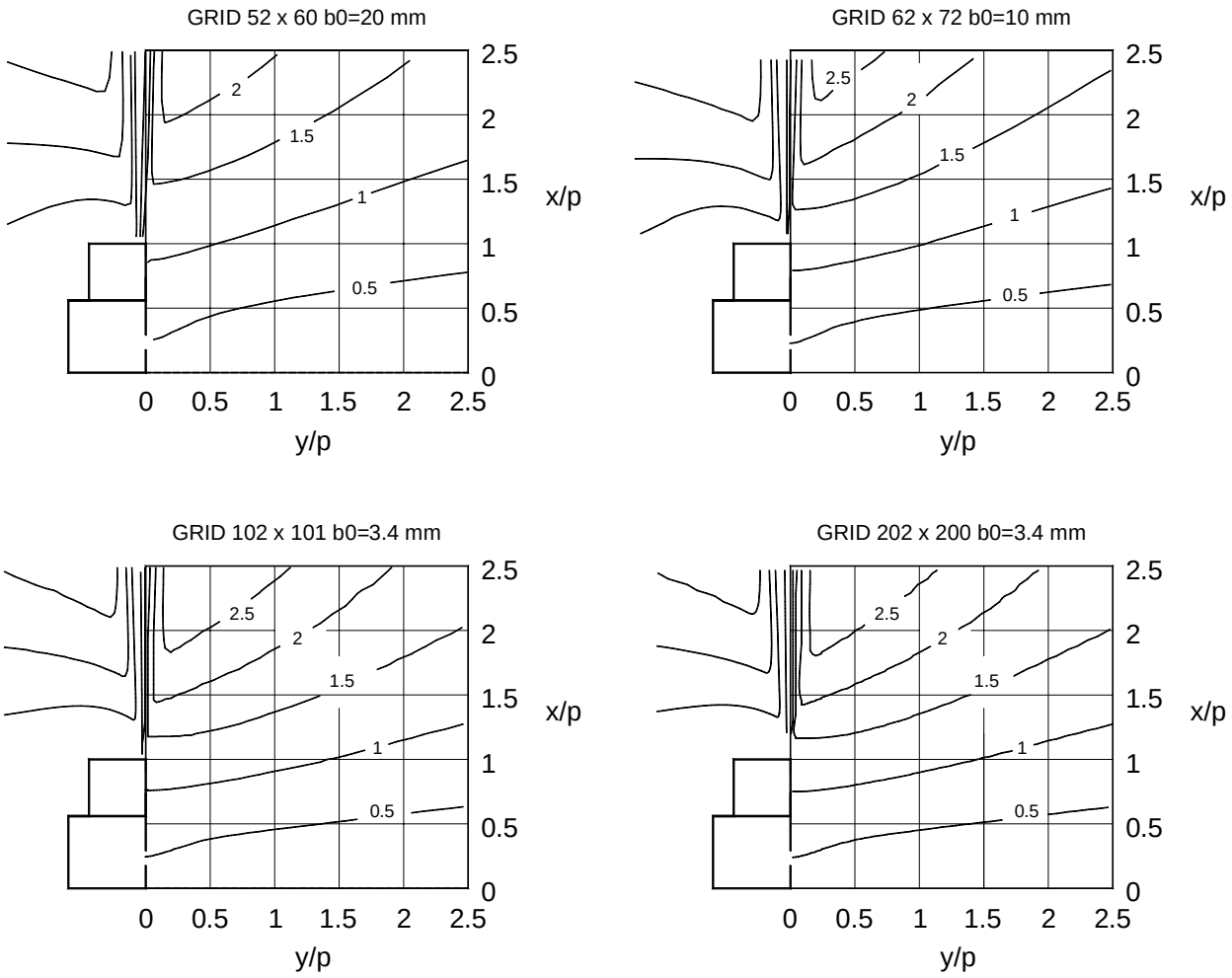

Figure 32. Calculated stream functions with various models when $G_f = 2.2$.

Table 1 gives a comparison of CPU time required for some typical calculations. The calculations with the basic model (b_0 = 3.4 mm) require much more CPU time than the other cases because the CPU time per iteration increased and the number of iterations needed for a converged solution was higher. It is apparent that by allowing small inaccuracies in the results the calculation times and thereby the calculation costs can be reduced drastically.

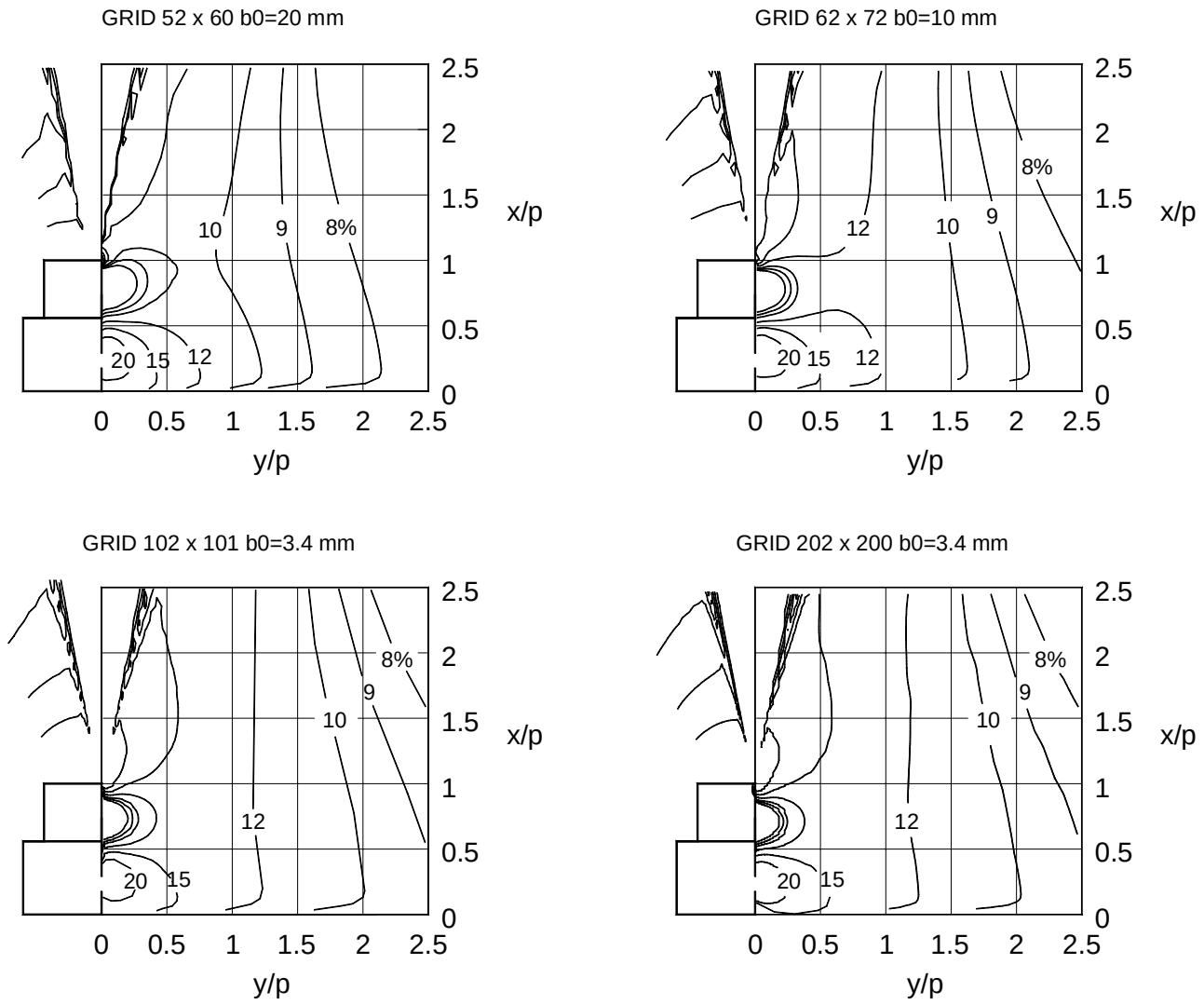

Figure 33. Calculated velocity contours with various models when G_f = 2.2.

Table 1. CPU times used in calculations.

Grid	Nozzle width (mm)	Total CPU time (min)
52 x 60	20	2
62 x 70	10	11
102 x 101	3.4	143

4.4 Short-circuiting flow

If the ratio of the jet momentum to the exhaust flow momentum is too low, the jet will bend towards the exhaust opening resulting in a short-circuiting flow. An example of the calculated stream functions and velocity contours for this situation are shown in Figure 34. The corresponding centreline velocities are shown in Figure 35.

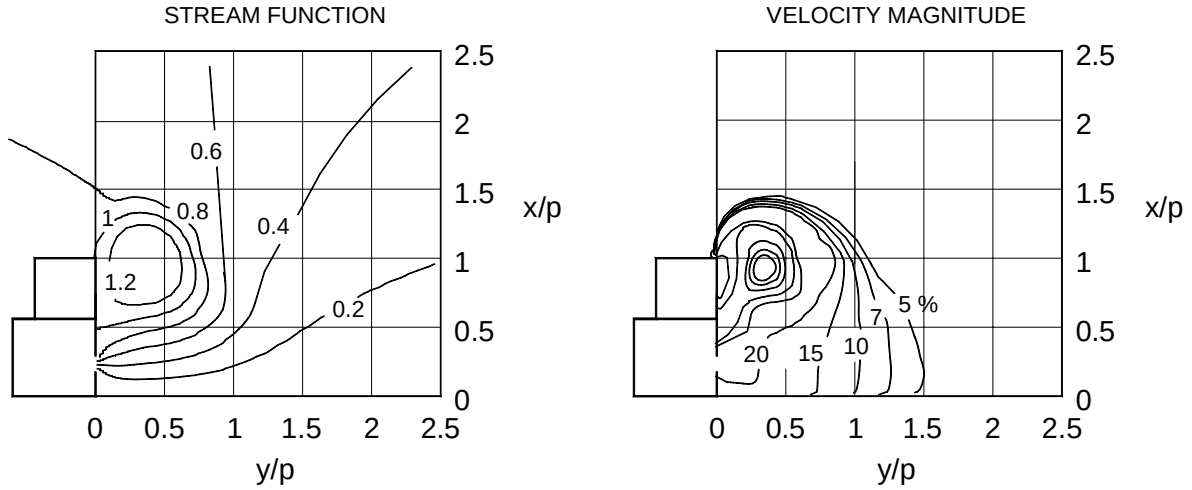

Figure 34. Predicted streamlines and velocity contours when G_f = 0.28.

Velocity contours and streamlines of Figure 34 show that the fluid just after emerging the jet outlet, is turning back and flowing towards the exhaust opening and that between the jet flow and the exhaust opening there is a small recirculation zone. This behaviour is in good qualitative agreement with smoke visualizations.

Contrary to an Aaberg hood working under designed operating conditions, with the short-circuiting flow the velocities are increased close to the hood, but further from the hood the velocities are almost unaffected. For example, the centreline velocity decreased to 10 % of the mean face velocity with conventional suction at y/p = 0.5 while with G_f = 0.28 this range was doubled (Figures 13 and 35). The capture efficiency measurements showed that the capture efficiencies were high (>95 %) over the entire measurement grid.

The short-circuiting conditions were observed with smoke visualization tests. In these experiments it was found that there is hysteresis in the short-circuiting conditions. When a short-circuiting occurred at a given jet velocity, a higher velocity was needed to recover from this situation. The corresponding lower and upper values of the operating parameter G_f, as a function of the exhaust flow rate, are presented in Figure 36. It is interesting to note that the short-circuit conditions were fairly constant and that the average value for the recovering flow was

G_f = 0.37 while the mean lower value was G_f = 0.25. The predicted short-circuiting flow conditions were between these values (Figure 36).

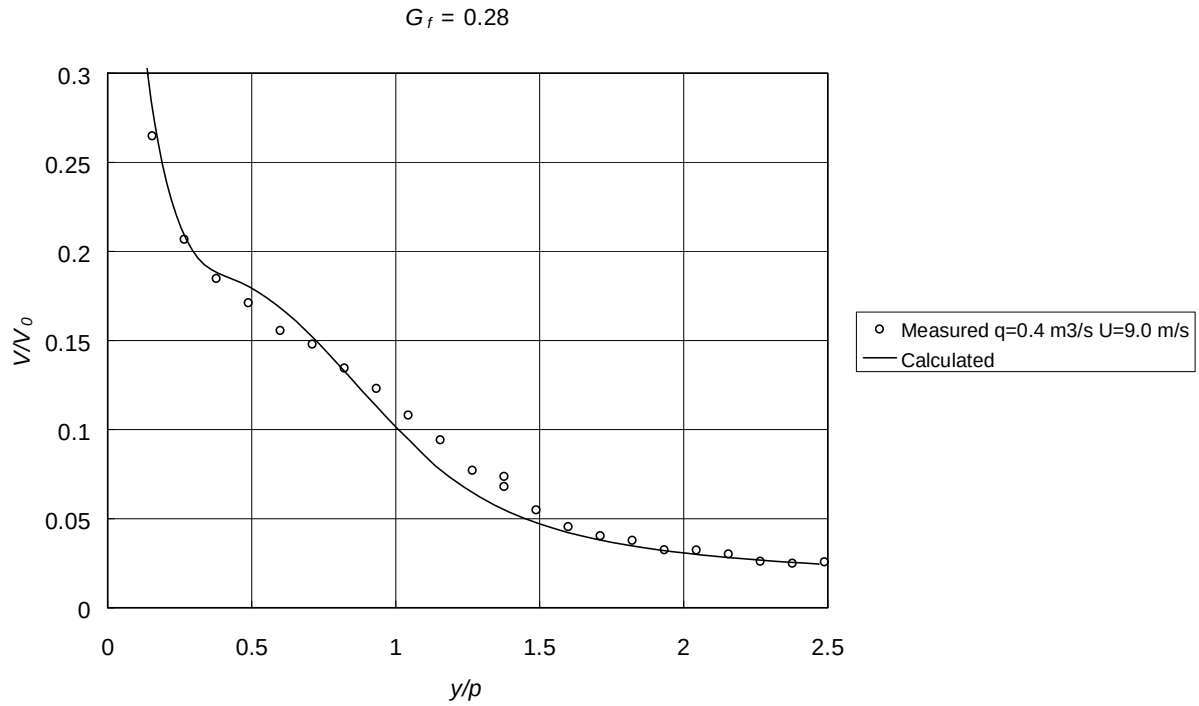

Figure 35. Measured and predicted centreline velocities when G_f = 0.24.

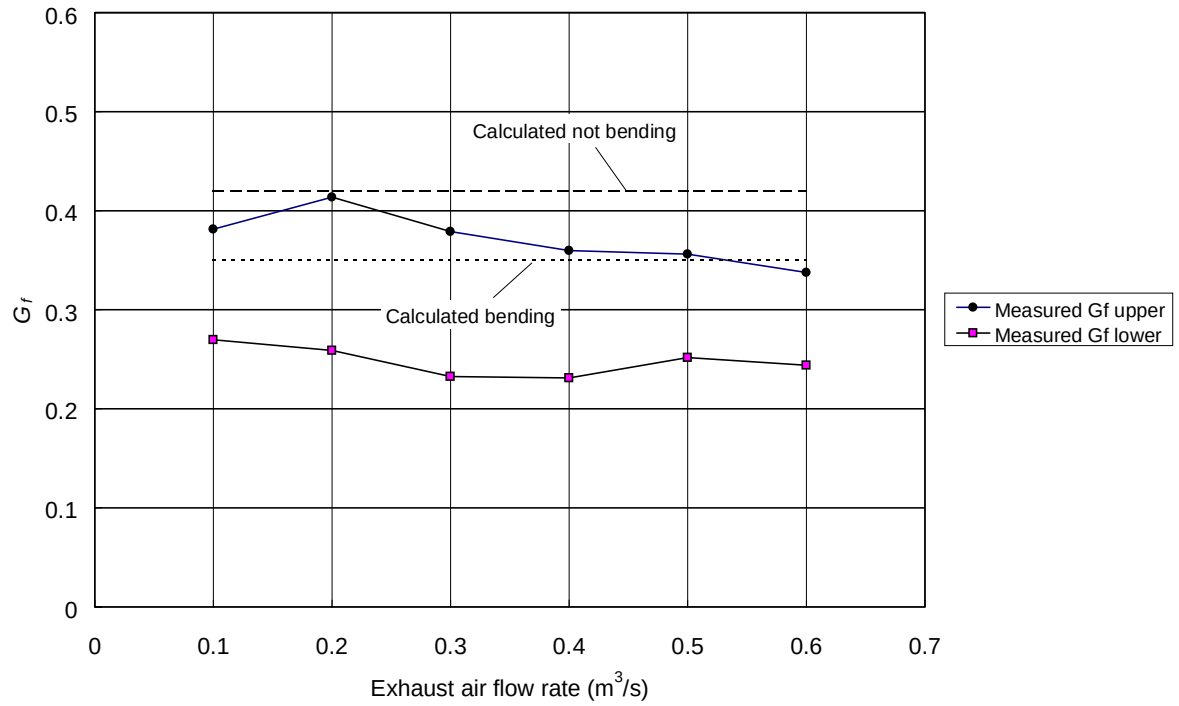

Figure 36. Observed and predicted conditions for the short-circuiting flow.

5 Conclusions

A significant increase in the velocity in front of the hood, especially at long distances from the opening, may be obtained with the use of a supply jet. For the desired performance, the supply flow must be properly balanced with the exhaust flow. Too weak a supply jet bends towards the exhaust opening while too strong a jet may result in a poor capture efficiency due to increased contaminant dispersion. During the experiments, the short-circuiting conditions could be avoided when the dimensionless operating parameter G_f was greater than 0.36. Overly high dispersion was avoided when G_f was less than 2.2.

The effect of the supply jet on the exhaust flow can be modelled with fairly good accuracy with both the potential flow and viscous flow models when the momentum of the jet is not exceedingly high. Both predictions become increasingly inaccurate in predicting the velocities as the strength of the jet increased. With appropriate approximations, the calculation times with the CFD model could be greatly reduced without altering the results significantly.

Contrary to the viscous flow model, the potential flow model can not predict the short-circuiting conditions. On the other hand, the calculation times and costs are much higher with full CFD models than with the analytical models. Moreover, the analytical model gives the most important parameters which affect the performance of these kinds of systems giving a possibility to understand the phenomena more thoroughly.

Jet enhanced exhausts offer an efficient way to increase the control range of exhaust systems. Further research is needed to evaluate the performance of Aaberg hoods in industrial applications.

6 References

Chen, C.J. and Rodi, W. (1980) *Vertical Turbulent Buoyant Jets - A Review of Experimental Data*. Pergamon Press, Oxford.

Flynn, M.R. and Ellenbecker, M.J. (1986) Capture efficiency of flanged circular local exhaust hoods. *Ann. Occup. Hyg.* **30**, 497-513.

Hogsted, P. (1987) Air movements controlled by means of exhaustion. In *Proceedings of Roomvent* '87, Stockholm.

Hunt, G.R. and Ingham, D.B. (1992) The fluid mechanics of a two-dimensional Aaberg exhaust hood. *Ann. Occup. Hyg.* **36**, 455-476.

Hunt, G.R. and Ingham, D.B. (1993) A mathematical model of the fluid-flow of a slot exhaust-hood reinforced by a two-dimensional jet flow. *Math. Engng. Ind.* **4**, 227-247.

Hunt, G.R. and Ingham, D.B. (1995) Long range exhaustion - a mathematical model for the axisymmetric air flow of a local exhaust ventilation hood assisted by a turbulent radial jet. *Ann. Occup. Hyg.* **40**, 171-196.

Hyldgård, C.E. (1987) Aerodynamic control of exhaust. In *Proceedings of Roomvent* '87, Stockholm.

Germann, L. (1991) REEXS - Reinforced Exhaust System. Ph.D. thesis, Danish Technological Institute (in Danish).

Saunders, C.J. and Fletcher, B. (1993) Jet enhanced local exhaust ventilation. *Ann. Occup. Hyg.* **37**, 15-24.

Schetz, J.A. (1984) *Foundations of Boundary Layer Theory for Momentum, Heat and Mass Transfer*. Prentice-Hall, Englewood Cliffs, New Jersey.

Schlichting, H. (1979) *Boundary Layer Theory* (7th Edition). McGraw-Hill, New York.